Surface-Induced Modification of Supported Late Transition Metal Complexes

Snezhkova, Olesia

2016

[Link to publication](#)

Surface-Induced Modification of Supported Late Transition Metal Complexes

OLESIA SNEZHKOVA
DEPARTMENT OF PHYSICS | LUND UNIVERSITY
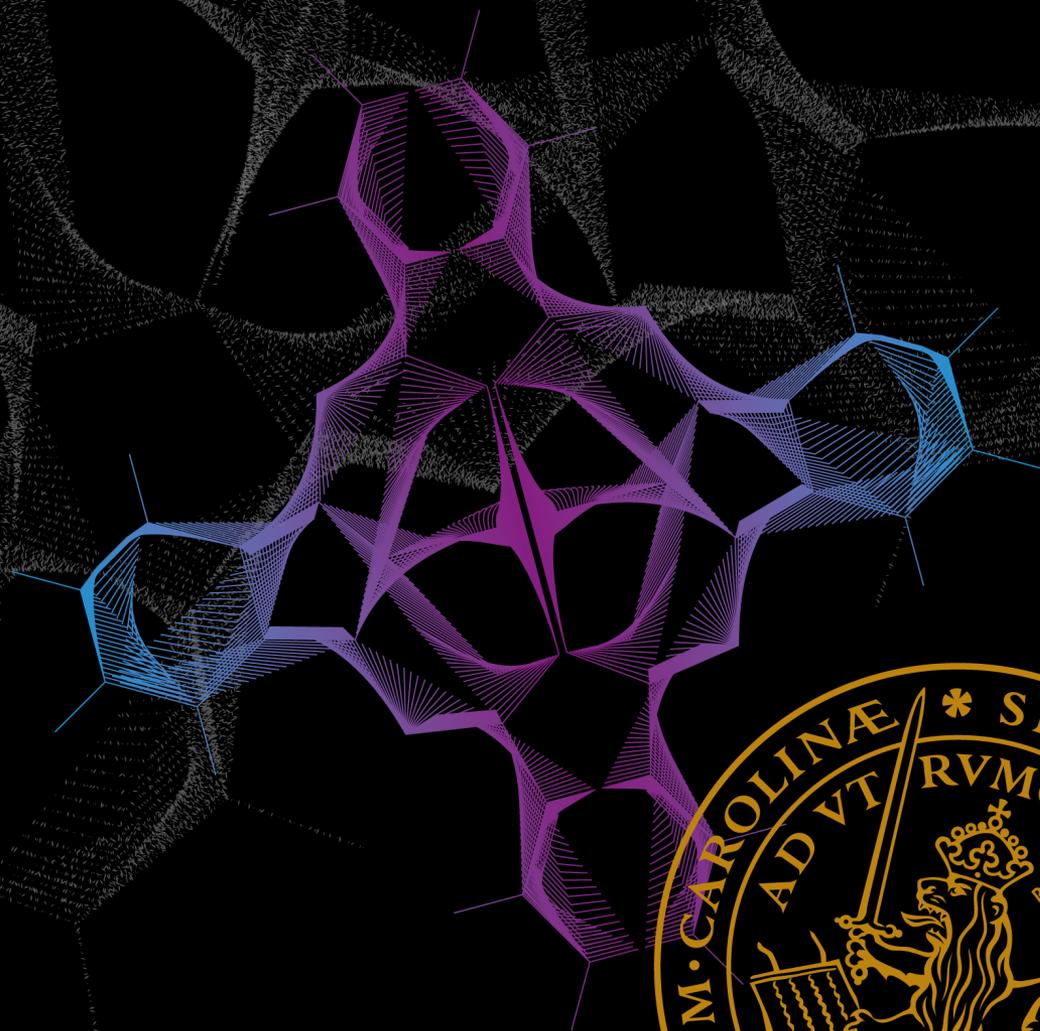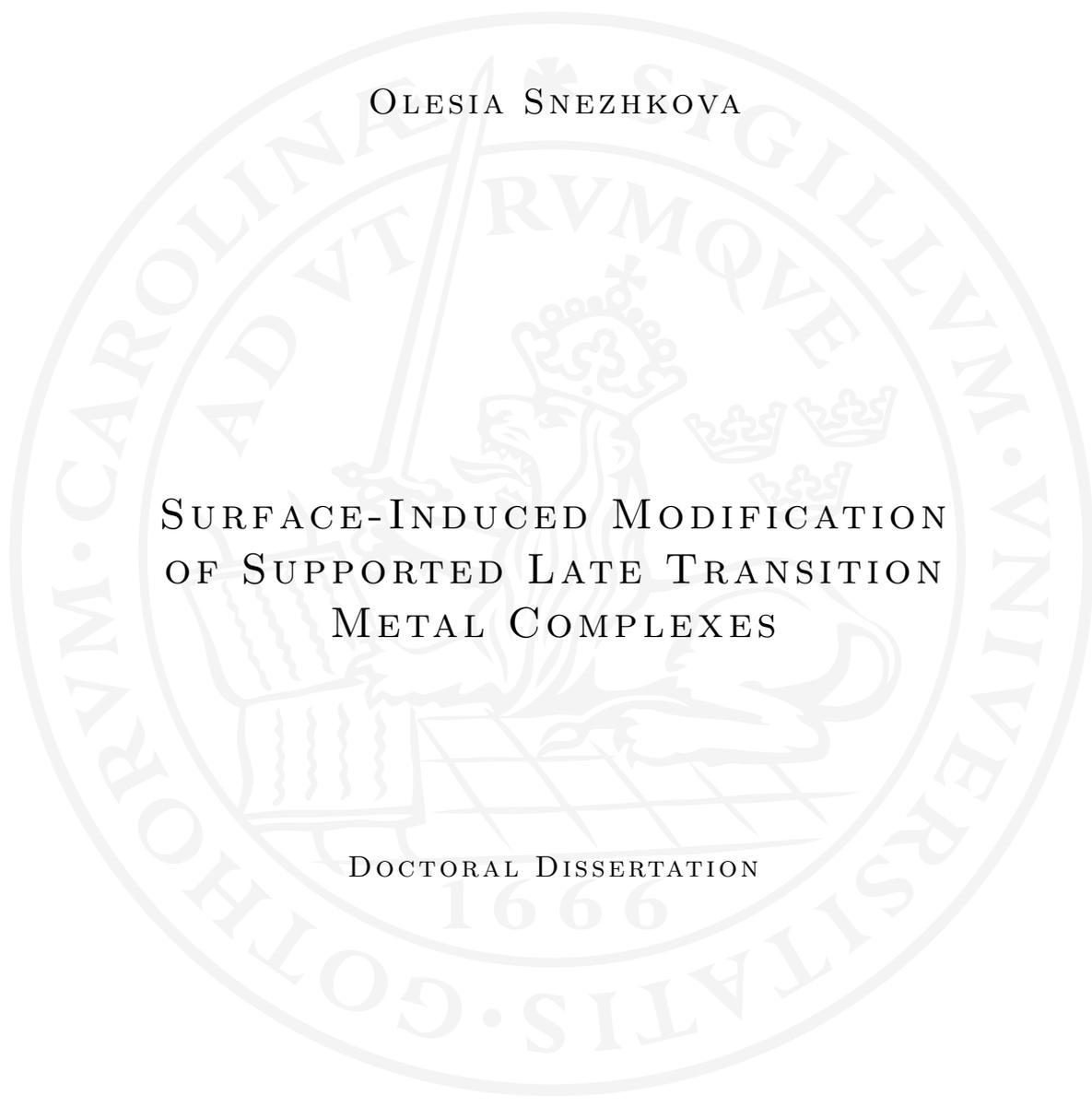
Olesia Snezhkova

Surface-Induced Modification of Supported Late Transition Metal Complexes

Doctoral Dissertation

Lund University

2016

Cover illustrations:
© Tomasz M. Kozłowski and Olesia Snezhkova

For those the most special, who inspired and caused it,

And you, who read this outcome of my scientific adventures.

Abstract

The work presented in this thesis addresses the investigation of the electronic, magnetic, and structural properties of late transition metal complexes supported on various surfaces. The research is aimed at studying the interaction between the molecules and the support, together with the intermolecular interaction. This knowledge is essential e.g. for the development of organic molecule-based devices and the creation of active and stable catalysts.

In this work, the modification of the electronic states of the iron phthalocyanine (FePc) complex induced by a Cu(111) surface was extensively investigated. These studies were motivated by the role that phthalocyanines play in charge injection devices and molecular electronics. The analysis revealed a non-isotropic charge transfer from the surface, which arises from the rehybridisation of molecular and metal electronic states and results in the breaking of the perfect fourfold symmetry of the molecule. In addition, I demonstrate a surface-driven thermal modification of the electronic and structural properties of the phthalocyanine molecules when deposited on Cu(111) support. This knowledge is essential because a thermal evaporation of adsorbates is the most common preparation technique for the creation of molecular monolayers. This technique is widely used for commercial purposes such as the creation of molecular switches and data storage devices.

The FePc molecule is also quite unique due to the similarity of its structural and magnetic properties to that of the reactive site in haemoproteine, a molecule known to perform the activation, storage, and transport of molecular oxygen. Therefore, I also investigated FePc as a synthetic model of the iron porphyrine in the haem reactive site. This investigation revealed that despite its structural similarity to haem, the molecule interacts with molecular oxygen only as a result of the stronger electronic coupling of the FePc molecules to the surface. These studies can help to obtain a better understanding of mechanisms of the haem–oxygen interaction.

Motivated by the success in the development and mass production of green and affordable surface-supported transition metal complex catalysts, this thesis incorporates the full characterisation of two new N-heterocyclic carbene palladium complexes anchored to a silica surface. The study is aimed at providing a comprehensive knowledge about stability, surface orientation, and catalytic activity of late transition metal complexes at surfaces for heterogeneous catalysis, as opposed to the more commonly used homogeneous catalysis in inorganic chemistry.

In summary, the strength of this thesis lies in the provision of a comprehensive overview of the interaction and surface-driven modifications of supported transition metal complexes on various surfaces and new insight into the magnetic and electronic properties of single molecules, monolayer, and multilayers.

Popular science summary

In our current world, the exponential growth in demand for smaller and faster devices leads to the fact that we will eventually face the problem that traditional semiconductor technologies will reach their limitation in terms of size and speed. Humanity's consciousness to tackle the global ecological issues in the next decade, will demand the substitution of all non-reusable and thus polluting industrial catalysts to environmentally-friendly and reusable ones. These problems can only be resolved from targeted science programmes, aimed at addressing the sustainable and environmentally friendly development of our society. The development of *molecule-based technology* represents a potential contribution to this ecological vision.

The field of molecule-based technology has developed in parallel with nanotechnology over the past decades. However, these systems can offer their own unique functional properties for prospective applications, compared to more traditional, hard condensed matter-based nanotechnologies. This is due to the small size, low cost, and structural perfection that molecules have to offer. The essence of their properties goes beyond classical physics, due to their quantum nature. This fact makes molecule systems as equally fascinating from a physics prospective as they are for their potential use in new device industries.

In the scope of this thesis, I investigate the properties of **supported transition metal complexes**. What are *transition metals* and what makes them so special? Most of the elements only use valence electrons - i.e., electrons that participate in the creation of chemical bonds, from their outer electron orbitals[1] to form bonds with other elements. Transition metals use the two outermost orbitals and, thus, have more valence electrons. This allows them to create bonds with many elements in a variety of shapes. All transition metals form stable compounds and depending on the amount of remaining valence electrons and their distribution in the outer orbitals can have different properties. The amount of borrowed or taken electrons by transition metal defines its unique properties, and is called oxidation number or oxidation state. Transition metals can have multiple oxidation states and knowing the oxidation state of the transition metal helps to determine the ability of the compound to react (exchange electrons and create bonds) with other species.

Transition elements tend to form complexes, i.e. molecules in which a group of atoms cluster around a single metal atom. The complexes discussed in this thesis contain *organic parts* that create a framework around the transition metal atom, which looses some electron density to this framework to become an ion species. *Organic* refers a carbon-containing compound, where carbon atoms in the form of rings or long chains can be attached to other atoms, such as hydrogen, oxygen, and nitrogen. The organic part of the molecule determines the amount of the given or obtained electrons and thus defines

---

[1]By orbital I imply the area within the atom where there is a high probability of finding electrons.

the electron properties of the compound. The most active part is the transition metal ion, which often - although not always - is responsible for all the interesting interactions with surrounding matter.

By varying the chemical environment of transition metal complexes, e.g. by placing them on different surfaces or adding different molecules, such as atmospheric gases or industrial products, one can change the density and distribution of the valence electrons in the metal centre of the molecule. In other words, the original properties of the complex and the electronic and magnetic properties of the complex are modified. The realisation that the electronic and magnetic properties of the transition metal organic compound can be tailored selectively has created a large diversity of possibile applications of these complexes. These include the creation of data storage devices, replacement of traditional semiconductor electronics, computer applications, gas sensing systems, as well as other applications.

One of the transition metal complexes which still holds attention of many scientists and engineers since its discovery almost 100 years ago is the **phthalocyanine** compound. The structure of this molecule is chemically very stable, such that many substitute species with unique properties can be synthesised. Phthalocyanines have been the focus of active research owing to their biological tolerance, semiconducting properties, possibility of manipulation of the electronic and magnetic properties, and due to their high light absorptivity. In view of the high demand of this compound in many different fields a knowledge of phthalocyanines' thermal, electronic, and magnetic properties is a essential.

In this work the iron phthalocyanine (FePc) compound has been deposited on different surfaces as a model system to investigate the application of metal phalocyanine molecules in electronic devices. This has been performed to study how the electronic and chemical properties can be tuned by depositing them on different types of supporting material.

In my work I show that the FePc molecule may take different electron densities from the surface depending on the support. This electron density can be unevenly distributed in the molecule and is also accompanied by a distortion away from its perfectly planar molecular structure. In this molecular distortion, two opposing parts of the molecule curve slightly upwards, while the other orthogonal parts bend slightly downwards toward the surface, in a so called *symmetry reduction* or symmetry breaking configuration. In my work the spectroscopic fingerprint of this effect has been demonstrated for the first time. The presence of a slightly higher electron density at one atom of the molecule decreases the energy required to remove an electron from the deeper orbitals of the atom, which is known as its binding energy. The presence of different amount of electron density on different atoms leads to the creation of several different binding energies and, consequently, the identification of a broader overall spectral line for the molecule.

In addition, the response to heating of the FePc molecules on the surface was also investigated. These studies were motivated by the preparation of molecular optoelectronic devices, where the evaporation of unwanted additional layers of molecules has been observed previously. Therefore, it is important to know how temperature influences the properties of the remaining single layer of molecules. My research shows that the increase of the temperature of the surface to the evaporation temperatures of FePc leads to irreversible processes during which most of the molecules merge together. There is

also some evidence that indicates that the molecules shorten the bond distance with the surface after this heat treatment process.

In this work FePc molecules are investigated not only from the scope of application in molecular electronics, but also from the perspective of gaining additional fundamental knowledge. The structural and electronic properties of the FePc molecules are very similar to that in active part of haem, the protein in the blood of all vertebrates responsible for activating, storage, and transfer of molecular oxygen. In this research, the FePc molecule is considered to mimic the active properties of haem. During my experiments I observed that the reactivity of the compound with respect to molecular oxygen changes depending on the nature of the surface the molecules are adsorbed on. My investigations can potentially help to create a better understanding of the mechanism of the biologically important haem-oxygen interaction.

The final part of this thesis is aimed at understanding the role of transition metal complexes in catalysis, a work of huge importance to both industry and ecology. Catalysts function by speeding up selected chemical reactions and thus lead to the increased production of a desired product. Catalysts function by either triggering reactions, or by making reactions occur at faster times and with less of energy consumption. Heterogenisation of transition metal catalysts studied here is advantageous for several reasons. Firstly, because they are supported on a surface, they are not consumed during a reaction. Secondly, only a small amount of the material is required to act as a catalysis. Thirdly, they are reusable and therefore cheap and ecological to use. Since supported transition metal complexes show very promising results in catalytic science, I have also investigated the properties of organometallic complexes with palladium as an active center.

The ultimate achievement of this thesis is its contribution to the understanding of the precise mechanisms of molecular manipulation, adsorption, temperature modifications, reaction sites and catalytic selectivity. The work presented here provides a solid foundation towards improvement in the development of smart design of catalytic materials and single-molecules electronic devices with better performance and lower cost.

CONTENTS

Preface

IV - Interaction of Cu(111)- and Au(111)-supported iron phthalocyanine with molecular oxygen at near-ambient and UHV conditions

Olesia Snezhkova, Ieva Bidermane, Roberta Totani, Shilpi Chaudhary, Luca Lozzi, Carla Puglia, and Joachim Schnadt

In manuscript

I was main responsible for planning and performing the experiments involving the Cu(111) sample, for the analysis of the results, and for writing the manuscript.

V - Structure, stability and catalytic activity in C-H activation of supported NHC-Pd complexes

Olesia Snezhkova, Ekaterina Bolbat, Fredric Ericson, Payam Shayesteh, Shilpi Chaudhary, Niclas Johansson, Ashley R. Head, Petter Persson, Ola Wendt, and Joachim Schnadt

In manuscript

I participated in planning and performing the experiments. I performed the analysis of the x-ray photoemission and absorption spectroscopy data and participated in the discussion of the theoretical results and their interpretation. I was main responsible for writing the manuscript.

List of papers not included to this thesis

VI - Controlled Short-Linkage Assembly of Functional Nano-Objects

Shilpi Chaudhary, Tripta Kamra, Khan Mohammad Ahsan Uddin, Olesia Snezhkova, H. Surangi N. Jayawardena, Mingdi Yan, Lars Montelius, Joachim Schnadt, and Lei Ye

Applied Surface Science, 300 (2014) 22

VII - Electrospray deposition of gold-loaded block copolymer reverse micelles onto a clean TiO$_2$ surface in vacuum

Ashley R. Head, Shilpi Chaudhary, Maria Messing, Florent Bacque, Niclas Johansson, Olesia Snezhkova, Tripta Kamra, Jesper N. Andersen, Joachim Schnadt

Submitted to Surface Science

VIII - Synchrotron-Based XPS Studies of Adsorption of (3-aminopropyl)-triethoxysilane on Rutile TiO$_2$(110) in UHV and at Ambient Pressure

Shilpi Chaudhary, Rocío Sánchez-de-Arma, Ashley R. Head, Niclas Johansson, Olesia Snezhkova, Tripta Kamra, Lars Montelius, Lei Ye, Fabrice Bournel, Jean-Jacques Gallet, Barbara Brena, Joachim Schnadt

Submitted to Journal of Physical Chemistry C

Abbreviations and symbols

AEY	Auger Electron Yield
AP XPS	Ambient Pressure X-ray Photoelectron Spectroscopy
BE	Binding Energy
CB	Conduction Band
CH	Core Hole
CT	Charge Transfer
DFT	Density Functional Theory
e^-	Electron
E_F	Fermi Level
E_i	Core Level
E_{kin}	Kinetic Energy
E_{vac}	Vacuum Level
FWHM	Full Width at Half Maximum
HOMO	Highest Occupied Molecular Orbital
HP XPS	High Pressure X-ray Photoemission Spectroscopy
$h\nu$	Photon Energy
IMFP	Inelastic Mean Free Path
KE	Kinetic Energy
LEED	Low Energy Electron Diffraction
LUMO	Lowest Unoccupied Molecular Orbital
NEXAFS	Near Edge X-ray Adsorption Fine Structure
Pc	Phthalocyanine
PEY	Partial Electron Yield
PES	Photoelectron Spectroscopy
RT	Room Temperature
STM	Scanning Tunnelling Microscopy
STS	Scanning Tunnelling Spectroscopy
TEY	Total Electron Yield
TD XPS	Temperature Dependent X-ray Photoelectron Spectroscopy
UHV	Ultra-High Vacuum
UPS	Ultraviolet Photoelectron Spectroscopy
UV	Ultraviolet
VB	Valence Band
XAS	X-ray Absorption Spectroscopy
XPS	X-ray Photoelectron Spectroscopy

CHAPTER 1

Introduction

"Small Is Beautiful", the phrase originating from the world of economics, politics and philosophy this time found its way to science and technology. Small is beautiful, because small is unique and small is affordable. The miniaturisation of technological appliances, pharmaceutical development, and huge progress in catalytic research have proven that not only a *single individual* can make a difference, but that also a *single molecule* can.

In the middle of the 20th century at the start of miniaturisation epoch Richard Feynman gave a groundbreaking lecture "There's Plenty of Room at the Bottom" [1]. During this talk Feynman fatherly smiled on the earlier technologies which were considered to have progressed far and considered the possibility of direct manipulation of individual atoms. He said, "The problems of chemistry and biology can be greatly helped if our ability to see what we are doing, and to do things on an atomic level, is ultimately developed - a development which I think cannot be avoided." At that instant the invitation to a new field was way ahead of its time and went unnoticed. Later, in the 1990s the article based on this lecture was re-discovered and re-published and gave a boost for interest in nanotechnology. Feynman suggested that the day we were to reach the peak of technological revolution would be the day we had learnt to control and manipulate matter at an atomic scale.

Nowadays nanotechnology is part of our everyday life, most of our everyday gadgets consist of nanometre-scale transistors, and an alternative field developing extensively right now is single molecule-based devices. Molecules have even more to offer, especially if one focuses on their use as small functional units. There are unique advantages molecules offer in comparison to nanometre-sized clusters and wires. These include: structural perfection and identity to each other, which allow to create the self-assembly of complex and functional superstructures; small size, making them good building blocks; synthetic tailorability, which implies that by varying the composition, geometry or by attachment of additional molecules to them [18, 23], one can tailor the electronic [26–32],

bonding [33], structural [34–38], and optical properties of the molecules, and also switch between two different quantum states of the molecule [60]. Organic molecules have shown beyond doubt that they are most promising for technological applications that offer a cheaper alternative to inorganic matter.

Despite all the advantages, the challenges of creating functional molecule-based devices are enormous. The use of molecules as functional units requires a full understanding and control of two factors: the intermolecular interactions and the interaction with the supporting surface. All the unique and useful molecular properties can be created, tuned, or destroyed depending on these two interactions. Thus, it is of paramount importance to fully study single molecules, their interaction in clusters, at monolayer and multilayer coverage, and with a large variety of interfaces. The work presented in this thesis addresses single molecules not only for their potential for application in molecule-based devices, but also with the aim of contributing to fundamental understanding. With this scope in mind I have investigated two types of transition metal complexes: metal phthalocyanine and N-heterocyclic carbene palladium complexes supported on different metal, semiconductor, and isolator surfaces.

Metal phthalocyanines

As Plato said, "science is nothing but perception", and there are many amazing examples of accidental discoveries. One of these is the discovery of phthalocyanine in 1928, created asa side product during the industrial production of phthalimide by a Scottish dye company [2]. In the process, which is driven by passing ammonia into molten phthalic anhydride stored in iron vessels, the traces of a dark blue substance were found. Due to its origin and the beautiful deep blue color, also known as Monastral blue or phthalo blue, the compound was named *phthalocyanine*. Despite the fact that the first record of phthalocyanine synthesis stems from 1907 [3], only in 1934 the compound was properly identified and named. This was the starting point for the long journey of investigation of the phthalocyanine's properties, a journey still ongoing.

In an series of papers the discoverers of the phthaloycanine compound, Linstead *et al.*, described the structure and main properties of the compound. They identified the presence of various metallic centres, which could not be eliminated by treatment with concentrated sulphuric acid [4–8]. This showed a surprising stability of the compound. In their work Linstead *et al.* proposed that the parent molecule possessed a macrocyclic structure formed by four isoindole units linked by azomethine bridges as shown in Fig. 1.1, later confirmed by X-ray diffraction by Robertson [9].

This initial work marked the start of an extremely extensive study of the physics and chemistry of this extraordinarily versatile compound which continues to the present day. The reason for the substantial interest in the compound is based in its fascinating properties, which also have lead to a widespread use. Perhaps the most obvious application of the molecule is as a dye molecule [10, 11], but its similarity to naturally occurring porphyrins is perhaps the most important characteristcis. As an example, in Photodynamic therapy (PDT), a treatment for cancer, porphyrin compounds were used. The injected molecules were shown to accumulate mostly in tumour cells. The
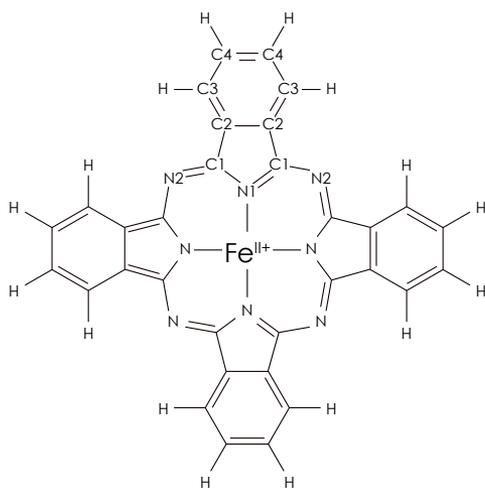
Figure 1.1: Schematic structure of iron (II) phthalocyanine ($C_{32}H_{16}N_8Fe$). There are two types of carbon and nitrogen atoms present in the structure. Carbon can be distinguished by either forming the outer benzene C=C rings (C2 (inner), C3 (middle) and C4 (outer)) or pyrrole C-N (C1) rings. Two types of structurally different nitrogen atoms can also be discerned: nitrogen forming the pyrrole rings (N1) and bridging aza-nitrogen atoms (N2).

photoexcitation of the compound, generated singlet oxygen as a result of the interaction between the ground state oxygen and the porphyrin triplet state, and led to localised tissue damage [12]. This technique was widely used until the 1980s, when it was shown that there were some serious complications associated with skin retention of the porphyrin molecules. Phthalocyanines were proposed as a substitute molecule in 1985 [13], and since then there has been considerable progress in the field [14–17].

More relevant for the work presented here, the structural and magnetic properties of phthalocyanine allow its use as a molecular mimics of certain metalloenzymes in biological environments [10]. One of such types of metalloenzymes are haemoprotein, which perform many important tasks in the bodies of mammals, involving the activation, storage, and transport of molecular oxygen. Therefore, it is of particular interest to investigate phthalocyanines as a synthetic model of iron porphyrin in the haemoprotein reactive site and perform measurements in realistic conditions. Thus, one of the scopes of the research work presented in this thesis is the investigation of the interaction of phthalocyanine with various ligand. Of special interest is to compare the molecule-ligand interaction of phthalocyanines adsorbed on different supports. It will be shown that the electronic structure of the molecule and its reactivity towards molecular oxygen – and presumably other molecules – can be changed significantly by the choice of surface.

Previous research has shown that the electronic and magnetic properties of the phthalocyanine molecule can be changed in various ways. Specifically, the spin state can be tuned to different values ($S \sim 0, 1/2, 1$), by adsorption of ligand molecules on top of the metal ion of the phthalocyanine compound [18–24]. In recent years the understanding has been broadened, and now there is ample evidence that the spin state and, in general, the electronic structure of the molecule can be modified by the choice of surface onto which the phthalocyanine compound is adsorbed [25–30]. Upon adsorption on different metal surfaces the molecules experience different electronic coupling to the support. Concomitant with the hybridisation of the molecular orbitals of the

compound with those of the surface is a charge transfer, which may induce, along with rehybridisation, a changed reactivity of the compound with respect to certain ligands. Here, specifically molecular oxygen has been studied. This result reveals how the iron phthalocyanine compound properties are different from those of haem, which opens for understanding the mechanism of haemoprotein interaction with molecular oxygen. As an additional consequence of the strong molecule-surface interaction and the charge transfer from surface to adsorbate [42–51] metal phthalocyanines(MPcs) adsorbed on primarily transition metal surfaces experience symmetry breaking. Previously, the effect has only been observed in scanning tunnelling microscopy (STM) images. As can be seen from Fig. 1.1, the gas phase molecule has a perfect fourfold (D_{4h}) symmetry, and thus metal phthalocyanines are expected to have a C_{4v} symmetry upon adsorption. However, this is not always the case as has been observed for MPc adsorbed on transition metal [31–41] and some isolator surfaces [52, 53], where the adosrbates undergo symmetry reduction towards C_4, C_2, or C_1 symmetries. It has been shown that whether symmetry breaking occurs or not is a function both of the metal center in the compound and of the support.

Extensive investigation of the interface between surface of support and MPc adsorbate is essential to obtain a detailed understanding of the physics and chemistry of the MPc-support interaction. Studies of the MPc adsorbed on different metal surfaces confirm a correlation between the charge state and molecular conformation [54, 55]. The electronic and magnetic properties are alternated due to a rehybridisation of the support and adsorbate electronic states and, partly, a charge reorganisation within the molecule-surface complex. This knowledge is crucial e.g. for building molecular nanodevices, such as molecular switches, data storage devices and molecular spin transistors [56–58]. This broad spectrum of applications of MPc compounds in molecular electronics is due to the large conformational flexibility of the compound [59], connected to a small but quite energetic nanomechanical motion. This makes it possible to use the compound for molecular switches and memories at the nanoscale [60]. Another example of surface-driven modification of the MPc's electronic and magnetic properties is the manipulation of the spin state of the molecule. It has been shown that it is possible to switch the spin of a single magnetic double-decker $TbPc_2$ on and off by shifting the molecular frontier-orbital energy by an STM pulse, which induces a rotation of the upper Pc macrocycle of the double decker [61]. This switching between two stable states is fully reversible and makes it possible to code information at the single-molecule level. All the applications and features mentioned above illustrate the critical role of a full understanding of the coupling of the MPc macrocycle with the support, which has been addressed in this thesis not only by plocal probe techniques (STM), but also by spectroscopy (XPS, XAS, UPS, and HPXPS).

The catalytic properties of phthalocyanine molecules have also risen interest [62], and various derivatives of phthalocyanine compounds are currently used for diverse catalysis applications. Examples are the photoreduction of water into hydrogen gas [63, 64], which would allow clean and energy efficient production of a renewable fuel; electro-oxidation reactions, that makes the molecule working as a electrochemical sensor [65]; use of phthalocyanine derivative as a catalyst for the detection of different thiols (in particular of homocysteine) in the human body [66]; and the reduction of oxygen to form new ligands, which is one topic addressed in the work presented in this thesis.

These and many other applications, together with the electronic and magnetic properties of phthalocyanine and the simplicity of synthesis of MPc, show how phthalocyanine has proven itself to be more than a simple dye molecule. The amount of research already invested in phthalocyanines has shown the importance of this compound for different research areas. Continued studies are vital so that full potential of these beautifully coloured molecules can be realised.

Here I present a study of the Fe phthalocyanine molecules on metal and semiconductor surfaces. The FePc molecules have been studied on Cu(111), Au(111), single layer of Cu_2N on Cu(111), and oxidised Cu(111) surfaces. For submonolayer and monolayer coverages of FePc, I investigate the impact of support and intermolecular interactions on the electronic and magnetic properties of the compound. I have performed an extensive study of surface-induced symmetry reduction of perfect fourfold symmetry of the molecule. Previously recorded by only means of imaging techniques, in my work symmetry reduction is mirrored in core-level photoemission spectra of the compound. I show that temperature treatment induces dehydrogenation and homocoupling of the molecules and reduces surface-molecule distance. I investigate how the single layer of copper nitride can cause a co-existence of Fe phthalocyanine with both high and low spin states of the iron ion, and how ligand attachment modifies these FePc with different spin states. In the work presented here I also study the reactivity of the FePc molecule with respect to molecular oxygen which can be tuned as a result of a stronger or weaker electron coupling to the surface.

Catalytic transition metal complexes

Catalysis is the process during which an additive can increase the rate of a chemical reaction without being consumed. This is achieved by the lowering of the activation barrier of the reaction. Life on earth is dependent on the catalytic activity of our enzymes, the macromolecular biological catalysts which carry out almost all the chemical transformations in living cells. Inspired by these processes, humans already for many years have tried to harness the tremendous potential of catalysts.

Catalysts can be either heterogeneous or homogeneous, depending whether they act in different or the same phase as the reactants. Homogeneous catalysis is the most commonly used in chemistry due to its high activity and selectivity, and this is where the transition metal catalysts are the most used. But despite its popularity due to high selectivity and molecular tunability, the technique has its limitations. It is hard to separate the catalyst from the product of reaction. The leaching of the catalyst and very often also thermal decomposition represent a huge drawback for homogeneous catalysis and often limit large-scale application in industry. Thus, many research groups are interested in the use of heterogeneous catalysts, were catalyst separation and absence of catalyst losses represent large advantages. As strong additional advantage, heterogeneous catalysts are environment-friendly and reusable, which also translate in reduced cost for industrial applications. Many unique catalysts have been discovered and reported in both industry and academia, and many research groups have therefore developed numerous number of ligands that can efficiently be employed in the catalysts associated

to transition metal.

N-heterocyclic carbenes are the most widely used ligands for the preparation of transition metal catalysts. The *NHC*-palladium complexes are widely used for many organic transformations. In particular, these complexes are well developed as catalysts for homogeneous catalysis. The next important step towards progress in catalysis is the combination of the advantages of both homogeneous (high activity and selectivity) and heterogeneous (catalyst separation, no catalyst losses) catalysis for transition metal complexes. One method combining these consist in the immobilisation of the homogeneous catalyst complexes on support materials, such as siliceous materials, metal-organic framework, or polymers. The development of the techniques for immobilisation of *NHC*-palladium complexes on surfaces is very promising, although it presents many challenges. One of them is the achievement of a stable surface binding while deactivation and dissociation of the supported molecules are avoided [68].

Following the interest for catalysis of supported metal ligand complexes [67], I have investigated the geometric properties, the stability and surface orientation, as well as the catalytic activity of two new *NHC*-palladium complexes immobilised on a silicon dioxide support (Fig. 1.2).
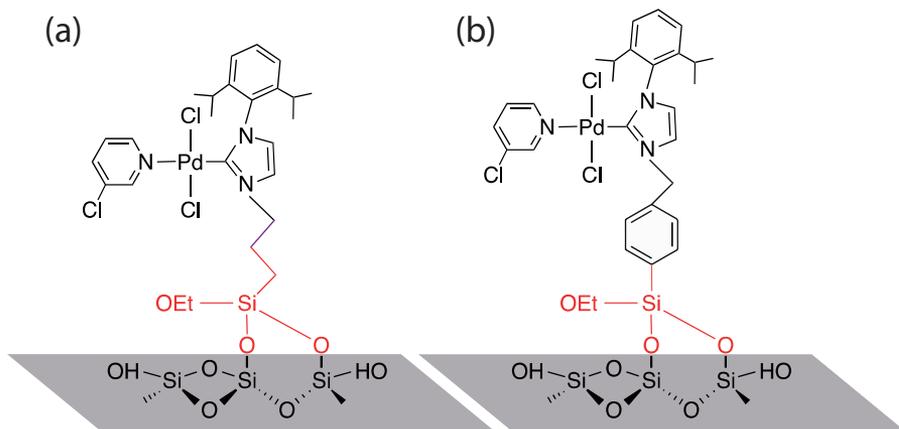
Figure 1.2: Schematic representations of a catalytic *NHC* (*N*-heterocyclic carbene) palladium complexes anchored to a silicon wafers through (a) a flexible linker and (b) a phenyl linker.

The research performed onto the immobilisation of *NHC*-Pd(II) complexes and discussed in this thesis a successful combination of chemistry, surface science techniques and theoretical models. Together, NMR, XPS, XAS, and DFT can give a proper insight into catalyst structure, stability, orientation of the catalyst on the surface and reactivity, and this has the potential to open the doors for many new commercial applications of supported molecular catalysts.

CHAPTER 2

Techniques for probing solid surfaces

The knowledge of surfaces and interfaces remains a prominent and developing science, important to both our fundamental understanding of nature and to many industrial and technological processes. However, the investigation of atomic-scale physical and chemical phenomena that occur at interfaces and surfaces is quite challenging. This is because surface studies require well-controlled experimental conditions and specially designed techniques, which are capable of providing detailed information on the chemical composition, geometrical structure, and electronic properties of a solid surface.

In this chapter, the instrumentation of the various surface science techniques exploited in this thesis are introduced. In order to gain a detailed insight into the physical and chemical nature of surfaces, a knowledge the atomic locations, electronic structure and bonding properties are essential. This thesis uniquely employs a combined spectroscopic and microscopic experimental approach, to provide complementary and corroborative characterisation of the surface properties. Furthermore, these experimental results are further enriched and placed into perspective by a theoretical analysis from our collaborators.

2.1   Electron Spectroscopy Methods

The science interest of surfaces and adsorbates has grown very significantly since its beginning in the 1970's, motivated by both pure scientific and technological considerations. From the many developed tools to investigate surface properties, one of the most powerful and widely used techniques exploit the detection of electrons emitted from the surface. The reasons for this attention is multifold: (i) at modest kinetic energies of some hundred eV, electrons have a short escape depth (only a few Å), which makes electrons excellent probes for surfaces, (ii) electrons are easy to focus since they are easily manipulated by electric fields, and (iii) electrons are easy to detect and count, and, moreover, electrons vanish after they have been detected (iv). However, the surface sensitive advantage of electron emission can also present a significant drawback in studies in the presence of certain gases and vapours, due to the electron's short mean free path and high scattering probability. In practice, this means that electron detection becomes a significant challenge in sample environment pressures below about 10^{-3} mbar.

The electron detection limit is not the only challenge is surface science, another problem arises from the fact that surface-sensitive electron spectroscopy measurements

requires Ultrahigh vacuum (UHV) conditions, with basic pressure of 10^{-10} mbar. The reason for this low pressure is that electron spectroscopy only probes a very thin layer at the surface of the sample. This is due to so called electron *inelastic mean free path* (IMFP), which is defined as the average distance travelled by an electron in a solid before it is inelastically scattered and is related to the mean escape depth (MED). As one can see in figure 2.1, in the kinetic energy range of interest, between about around 10 and 2000 eV, the IMFP is of the order of a few Å [69] (probing depth). Therefore it is highly important to achieve conditions in which atomically clean surfaces can be preserved for the duration of the experiment. These conditions can be achieved in vacuum better than 10^{-10} mbar for most of the materials, including the most reactive ones like alkali or rare earth materials.
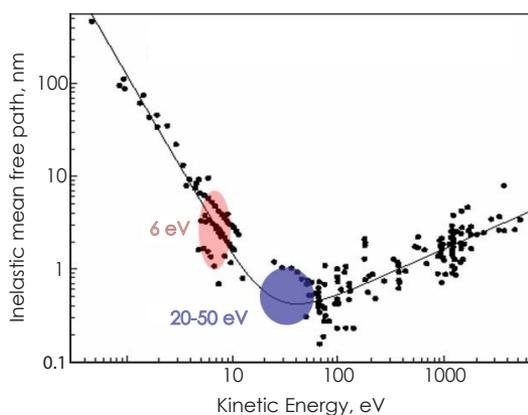
Figure 2.1: Electron mean free path for various metals as a function of kinetic energy [69]. The minimum of the escape depth (2-5 Å) is found for a kinetic energy of around 20-100 eV. Image is modified from ref. [69].

One of the most widely used electron-based surface analysis techniques is Photoelectron spectroscopy (PES). This technique is based on the photoelectric effect, discovered by H. Hertz in 1887 during experiments with a spark-gap generator, the earliest form of a radio receiver and was later theoretically explained by A. Einstein in 1905, for which he was awarded the his Nobel Prize in for Physics in 1921. He introduced the quantum hypothesis for the photon to arrive at the relationship between photon energy and electron kinetic energy.

In the energy range of interest, the photon-electron interaction can be described by photoemission (Fig. 2.2 (a) and (b)) and photoabsorption (Fig. 2.2 (d)). The excited system decays in subsequent events (Fig. 2.2 (c)). In X-ray Photoelectron Spectroscopy (XPS), for which the energy of the incoming photon is in the soft X-ray regime (100 to > 2000 eV), the photon is absorbed by an atom, leading to the emission of an electron from either the valence or an inner shell (Fig. 2.2 (b)). By contrast, in Ultraviolet Photoelectron Spectroscopy (UPS), absorption of the photon (5 to 100 eV) can only lead to emission from valence or shallow core levels of investigated material. In either case, the process leads to an ionised final state (Fig. 2.2 (a)).

The absorption of a photon with well-defined energy E, by an atom, leads to ionisation and the photoemission of an electron, provided that the photon energy is well above the absorption threshold (X-ray photoemission spectroscopy). If the photon energy is close
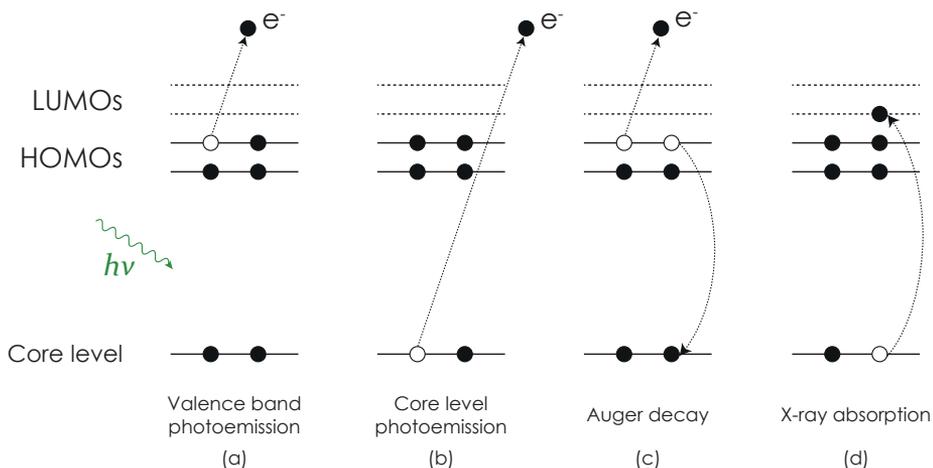
Figure 2.2: Schematic of the photon-electron interaction. In valence band photoemission (a), an electron from the valence band is promoted into the vacuum (in UPS or XPS); (b) the same kind of process takes place in core level photoemission, but necessitates absorption of a higher energy photon (XPS only); (c) Auger decay process; (d) X-ray absorption process.

to the threshold, an absorption process into the unoccupied states of the sample may take place (X-ray absorption spectroscopy).

2.1.1 Theory of X-ray Photoemission Spectroscopy

In photoemission, the kinetic energy (E_{kin}) distribution of the photoelectrons is measured by an electron energy analyser and a photoelectron spectrum is recorded. The binding energy (BE) can be determined from energy conservation:

$$BE = h\nu - E_{kin} - \phi, {}^{[1]}$$ (2.1)

where ϕ represents the work function of the sample. The technique was developed by Kai Siegbahn and his co-workers at Uppsala University [71]. For "for his contribution to the development of high-resolution electron spectroscopy" Siegbahn was awarded the Nobel Prize in 1981 [72].

Photoelectron spectroscopy measures the electron states of a sample, and in XPS one typically is most interested in the core levels. The exact energy of the photoemitted electrons depends not only on the elements that constitute the sample, but also on their chemical state (see also below) and can therefore be used for chemical analysis. Hence, another name for XPS is Electron Spectroscopy for Chemical Analysis (ESCA) [73].

---

[1]This formula is only valid for a metallic sample. For semiconductors the work function can be determined only in case if the sample is sufficiently conductive to record its Fermi level [70], otherwise the vacuum level is used. There is no work function for free atoms and molecules.

An x-ray photoemission (XP) spectrum displays the number of collected electrons as a
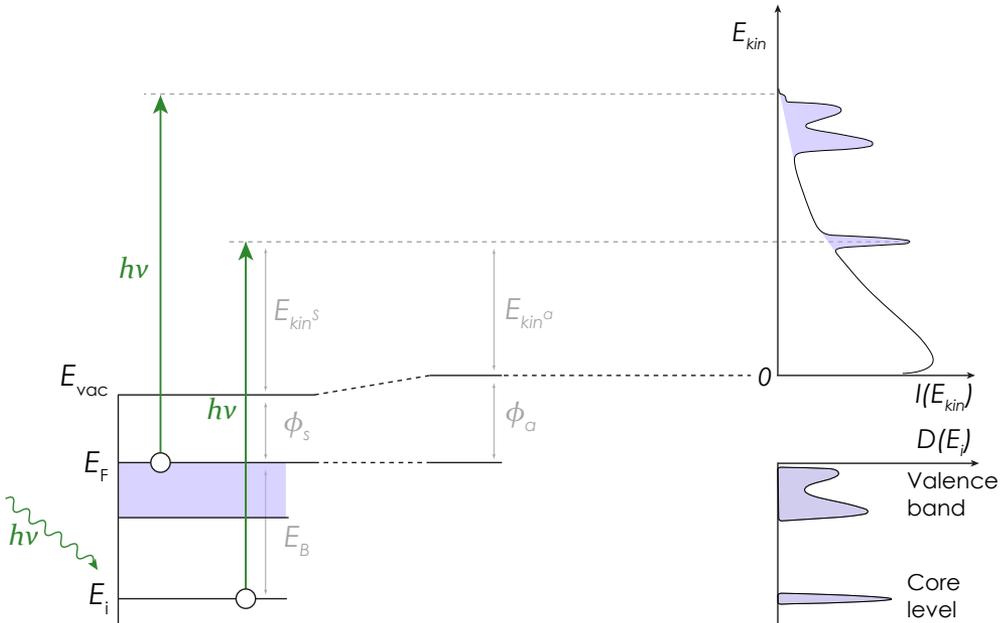
Figure 2.3: Schematic of the energy level alignment in photoemission of a conductive sample in electrical contact with the electron energy analyser, thus the Fermi levels of the system are aligned. The diagrams show the correlation between the photoemission spectrum at a certain kinetic energy $E_{kin}(h\nu)$ and the density of states of the sample $D(E)$. Image is modified from ref. [74].

function of kinetic energy (Fig. 2.3), which can be recalculated to binding energy. The basic idea is that the binding energy of a photoemitted electron is element-specific and also specific for every energy level inside an atom. Moreover, it can be affected by the nature of its chemical environment, as observed by a small shift in the energy position of the photoemission line.

In figure 2.3 the photoemission spectrum is represented by a distribution $E_{kin}(h\nu)$. The peaks of elastically scattered photoelectrons, which do not loose energy in collisions with other electrons on their way to the surface and the vacuum, are superimposed on the continuous background of inelastic secondary electrons [74]. The background intensity at low kinetic energies increases, since most photoelectrons undergo many inelastic losses and finally, a lower kinetic energy.

As shown in figure 2.3, since sample and spectrometer are in contact and thus their Fermi levels aligned, the binding energy can be calculated using the kinetic energy measured by the electron energy analyser

$$BE = h\nu - E_{kin^s} - \phi_s = h\nu - E_{kin^a} - \phi_a. \tag{2.2}$$

For a precise determination of the binding energy one needs to calibrate $h\nu$ and ϕ_a. For the metallic sample this can be achieved by measuring both the kinetic energy of core level and Fermi level. The binding energy of the core level relative to the Fermi edge therefore is given by the energy difference between these two spectra.

Quantum Description of the Photoelectric Effect

Photoionisation of the target atom, caused by an incident quantum energy $h\nu$ of X-rays, removes an electron from a K shell in the atom and thus leads to the emission of characteristic K shell radiation.[2] In quantum mechanics the particle's **wave function** $\psi(x,t)$ is determined, which defines the *probability* of finding the particle at point x, at time t. This can be achieved by solving the Schrödinger equation, which plays a role logically analogous to Newton's second law: for given initial conditions ($\psi(x,0)$), it determines $\psi(x,t)$ for all future time [75].

In its simplest form, quantum mechanics treats the photoemission process as a time-dependent perturbation problem. It is concerned with finding the changes in the discrete energy levels and eigenfunctions of a system when a small disturbance in the form of an incident x-ray quantum is applied. The Hamiltonian is split into two parts, $\widehat{H} = \widehat{H}_0 + \widehat{V}$. By assumption, the Schrödnger equation involving $\widehat{H}_0$ without perturbation can be solved exactly numerically: the eigenfunctions and eigenstates are thus known. However, the interesting part is $\widehat{V}$. In the time-dependent perturbation theory the light interaction is considered as a "perturbation" and the aim of the theory is to determine how this perturbation influences the energy of the system.

Since the Hamiltonian H is time-dependent, there are no stationary solutions of the Schrödinger equation

$$ih\frac{\delta\psi}{\delta t} = H\psi \Longrightarrow ih\frac{\delta}{\delta t}\mid\psi(\mathbf{r},t)\rangle = (\widehat{H}_0 + \widehat{V}(t))\mid\psi(\mathbf{r},t)\rangle \tag{2.3}$$

so that energy is not conserved. Therefore one should calculate approximately the wave function ψ and base calculations of the interaction Hamiltonian on justified approximations.

The photoemission process produces a final state that is lacking one electron with respect to the initial state. Therefore, the basic excitation process can be described according to

$$\overset{\text{Initial state}}{\psi_{tot}^i(N), E_{tot}^i(N)} \overset{h\nu}{\longrightarrow} \overset{\text{Final state}}{\psi_{tot}^f(N,K), E_{tot}^f(N,K),} \tag{2.4}$$

where $\psi_{tot}^i(N)$ (further - $\psi^i(N)$) is the initial-state N-electron wave function with a total energy $E_{tot}^i(N)$ and $\psi_{tot}^f(N,K)$ is the Kth final-state N-electron wave function, including the photoelectron, with a total energy of $E_{tot}^f(N,K)$ [104]. The index K describes all modes of excitation possible within the final state in an orbital k (translational, electronic and vibrational).

---

[2]In this simplified model I do not consider any secondary excitations.

To solve the full Schrödinger equation the $\widehat{V}$ component can be simplified in the *electric dipole approximation*. The approximation presumes that the wavelength of the exciting electromagnetic radiation is much larger than the atomic dimensions. The interaction Hamiltonian is then given by the dipole operator D which is defined as the summation of the product of the charge times the position vector for all charged particles involved ($\sum_{N} q_N r_N$). Then the **transition probability** per unit time, ω, corresponding to the transition to a group of final states, can be found to the first order in perturbation theory as [77, 78]

$$\omega = \frac{2\pi}{\hbar} |\langle \psi^f(N) \mid D \mid \psi^i(N) \rangle|^2 \rho(f). \qquad (2.5)$$

Here, $\rho(f)$ is the density of final states. This formula, first derived by P. A. M. Dirac and later dubbed by E. Fermi as 'Fermi's Golden Rule' of perturbation theory. Fermi's golden rule has wide applications in quantum physics, but the present purposes, it can be employed for to calculate transition rates, photocurrents, absorption cross sections, and spectral functions. The transition probability from the initial state to the final state $i \rightarrow f$ (i.e. the probability that the system, initially in the state i, be found in the state $f \neq i$) can be written as [79]

$$\omega \propto \frac{2\pi}{\hbar} |\langle \psi^f(N) \mid D \mid \psi^i(N) \rangle|^2 \delta(E^f(N-1) + E_k - E^i(N) - h\nu). \qquad (2.6)$$

In equation 2.6, δ function ensures energy conservation, meaning that the photon energy needs to be equal to the difference between the final state $E^f(N-1) + E_k$ and initial state $E^i(N)$ for photoionisation to happen. The $|\langle \psi^f(N) \mid D \mid \psi^i(N) \rangle|$ is a **transition matrix element**.

If one additionally applies a *one-electron view* of the photoemission process, in which one considers only one-electron wave functions and thus separates the orbital involved in the photoionisation from remaining electrons, then the transition matrix element can be rewritten as

$$\langle \psi^f(N) \mid D \mid \psi^i(N) \rangle = \langle \phi^{f,E_k} \mid D \mid \phi^{i,k} \rangle \langle \psi^f(N-1) \mid \psi^i(N-1) \rangle. \qquad (2.7)$$

Here the initial wave function $\psi^i(N)$ is rewritten as a product of the one-electron wave function of the orbital from which the electron was emitted $\phi^{i,k}$ and of the wave function of the remaining $N-1$ electrons after photoionisation $\psi^i(N-1)$. Similarly, the final state wave function is rewritten as a product of the wave function of the photoemitted electron ϕ^{f,E_k} and the many-electron wave function $\psi^f(N-1)$ of the remaining ion after photoionisation. The matrix element is thus a product of a one-electron matrix element and an $(N-1)$-electron overlap integral [79].

To obtain chemical information on the sample, one needs to estimate the (relative) photoelectron binding energy peaks positions and compare them to the experimental results. Using energy conservation (equation 2.2), the binding energy corresponding to

leaving the ion in a state described by $\psi^f(N-1, K)$ can be expressed as

$$E_b(K) = E^f(N-1, K) - E^i(N). \tag{2.8}$$

This definition is exact and the most useful theoretical tool in analysing XP spectra. This implies that total energies need to be calculated and this is usually performed by density functional theory (DFT).

Simpler approaches justify cruder approximations and one of the most well known is the *frozen orbital approximation*. In this approach, the orbitals of the photoionised atom are considered to be unaffected by photoionisation process. For the calculations of ionisation energy during photoemission process the Koopmans' theorem is used. This states that that the binding energy of the electron before emission is equal the negative Hartree-Fock energy of the orbital from which the electron is emitted. The electrons remaining in the system are considered to be unaffected by the photoionisation, meaning that $\psi^{f,Koop}(N-1) = \psi^i(N-1)$, which renders the overlap integral unity (eq. 2.7). Therefore, the transition matrix element is built on the one-electron wave functions. However, Koopmans' approximation neglects all relaxation energies.

$$E_b^{Koop}(k) = -\epsilon_k = E_f^{HF}(N-1, k) - E_i^{HF}(N), \tag{2.9}$$

The Hartree-Fock method for calculating the energies of a multi-electron system is based on the statement that the wave function of an N-electron system can be approximated by a sum of Slater determinant of N orthonormal one-electron spin-orbitals (*one-electron view* discussed above). Using Slater determinants ensures that the total electronic wave function of the systems is antisymmetric with respect to exchange of any two electrons and thus obeys the Pauli exclusion principle.
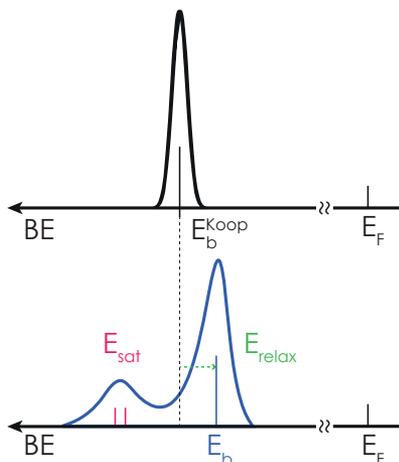

Figure 2.4: Models of the atomic response to photoionisation: (above) frozen orbital approximation and (below) Koopmans' binding energy corrected to relaxation energy E_{relax} and additional final state contributions E_{sat}.

According to Koopmans' theorem, the photoemission spectrum would always consist of single lines. In reality, however, the orbitals are not frozen, and to relate Koopmans' energies to the binding energies actually measured one has to correct for the *relaxation energy*. This is the amount of energy necessary for the adjustment of the whole system to the hole left upon photoionisation. The relaxation shifts the binding energy by E_{relax} towards lower binding energy and it occurs both in emitting atom and surrounding atoms upon ionisation. Additionally, in the system will appear interactions by the response of the system to the core-hole potential, leading to convolution of the bare core line with additional lines (satellites) (see figure 2.4) [79]. Therefore, for achieving a more accurate estimation of the binding energy, one has to consider additional final state contributions, such as relaxation, relativistic, and correlation effects [80, 104].

$$E_b(k) = -\epsilon_k - \delta E_{relax} + \delta E_{relat} + \delta E_{corr} \tag{2.10}$$

It is important to remember that the first moment of the spectral intensity remains unchanged and is located at Koopmans' binding energy. This statement is based on the so-called **sudden approximation**, which states that the response of the system to the creation of the photohole is instantaneous and that there is no interaction between the phtoemitted electron and the remaining system. Within this approximation an important 'sum rule' can be derived. It states that the average of the binding energies peaks (E_b and E_{sat}), which are associated with a primary excitation is equal to Koopmans' theorem binding energy $-\epsilon_k$. Thus, in the sudden approximation, the position of the Koopmans' energy peak corresponds to the first moment of the entire spectrum including the satellites (Fig. 2.4).

Core level shifts

In a some ways, core levels of atoms can be considered as fingerprints of atomic systems. Thus, the observation of the changes of their relative position, *i.e.* of *core-level shifts*, allows to analyse modifications of atom caused by the environment surrounding this atom. Interestingly, despite the localised nature of core level electrons and their irrevelence in the formation of chemical bonds, any change in the electron distribution of the valence levels affects the core level binding energies, which results in so-called **chemical shifts**.

The most common definition of chemical shifts is only related to initial-state effects, although, for some materials, such as metals and metallic surfaces, the final-state effects are also important [81]. Thus, both initial and final states influence on core-level shifts are described here.

Initial state core level shifts. In 1924 Lindh and Lundquist [82] discovered the effect of chemical combination on X-ray line spectra. Since their discovery numerous studies have been reported, illustrating how emission X-ray line changes under influence of valence charge [83, 84]. In theory, valence electrons penetrate the ion core for less than 10% of that of their probability distribution. When they happen to be inside of the core, their charge repels the charge of the core, therefore they *screen* partially the core electron-nucleus attraction and the binding of the core level is reduced. If the atom forms bond, some of the charge is removed or transferred from the atom and

consequently, the screening is reduced. This effect results in the core electrons being more strongly attracted to the nucleus and consequently an increase of absolute value of binding energy. Thus all inner levels of atom are shifted by a few eV when the valence electron configuration changes.

A special case of chemical shift is a *surface core level shift*. The core-level binding energy of surface atom is different from that of a bulk atom due to the different environment of the atoms. By performing energy dependent measurements one can in principle assign different bulk and surface contributions in a photoemission spectrum.

The presence of adsorbates on the surface additionally changes the electronic configuration of the system and a magnitude of these shifts is connected to the interaction strength of adsorbate-surface system. In the case of strong bonding of adsorbate to the surface, a charge transfer from/to the surface may occur.

Final state core level shifts. There are different types of final state contributions to core level binding energy shifts. One of them is the relaxation of atom or molecular orbitals upon creation of a core hole, also known as *core-hole screening*.

The other type of contribution is an *image charge* screening. In the case of weak adsorption (physisorption) on metal surface, the creation of a core hole, *i.e.* positive charge, in adsorbent is accompanied effectively by the simultaneous creation of a negative charge in metal surface, which reduces the ionisation potential [85]. Depending on a response time scale, it either alters the position of the core levels or maybe observed as a satellite structure (also discussed in the section below). In the case of strong bonding, the creation of a core hole is often involves a charge transfer from/to the adsorbate, so-called *charge transfer* screening. Both, image charge and charge transfer screenings involve a charge redistribution in order to achieve a totally neutral core hole site.

Contributions to Line Shapes of Photoemission Spectra

There are various effects and factors which determine the line shape of a core-level spectrum. The observed energy distribution can be viewed as a convolution of the fundamental spectral shapes connected to these processes. In order to obtain quantitative details and extract information from a core-level spectrum, one needs to understand the nature of all of the individual contributions.

During the electron photoemission process, the line-shape is represented by the main core level photoemission peak accompanied by additional lines (satellites) which occur due to the response of the atomic system to the created core-hole potential. **The main photoemission line** can have different broadening mechanisms. In the case of adsorbate on a surface, it is mainly broadened due to collective excitations in quantised vibrations in the solid lattice (vibrational excitations). There is also a finite broadening due to the experimental resolution [86, 90].

The vibrational effects occur due to the fact that the potential energy curves of the atomic motion are different before and after ionisation process. According to the *Franck-Condon principle*, the relative transition probabilities of the electronic transition is given by the overlap between the initial and final state nuclear motion wave functions. The transitions between vibrational levels are favoured when they correspond to a

minimal change in the nuclear coordinates. For a free molecule the number of modes to be excited is limited, therefore the final vibrational excitations can be described in terms of discrete states. For solids, on the other hand, the atomic motion can be treated as phonons, [89] which create a continuous broadening function that often can be considered to be of Gaussian shape. Thus, for solids a Gaussian distribution can be used to account for the broadening of the main photoemission line due to both, instrumental and phonon broadening. For a symmetrical Gaussian function, the relation between intensity and energy is given by

$$I_G(E) = I_0 exp(-\frac{ln2(E_0 - E)^2}{\omega_G^2/4}).$$ (2.11)

Here, ω_G is a Gaussian FWHM, E and E_0 are the kinetic energy of the emitted photoelectrons and energy position for the maximum intensity I_0 of the peak, respectively.

A Lorentzian function is used to include the core-hole finite life-time. In the scope of this thesis as I work with solid surfaces, where the core-hole life-time broadening is considered to be negligible. Although, I briefly mention it here because a combination of Gaussian and Lorentzian broadening results in a pseudo-Voigt function, which is the most appropriate for fitting complicated, overlapping line-shapes and has been used widely in the work presented here.

A spectral line cannot be infinitely sharp as a consequence of Heisenberg's uncertainty principle $\Delta E \Delta t \geq \hbar$, which dictates that the energy level of an excited state of an atom can never be determined precisely because of finite lifetime of the hole state [87]. Thus, the line shape is broadened over a ***natural line width*** with Lorentzian shape and the relation between intensity and the energy can be represented by following relation

$$I_L(E) = I_0(\frac{\omega_L}{2})^2 \frac{1}{(E_0 - E)^2 + (\omega_L^2/4)}.$$ (2.12)

Here ω_L is Lorentzian full width at half maximum, E is a kinetic energy of the out-coming electron, and E_0 is the energy position for the maximum intensity of the peak (I_0).

Satellites. In reality samples are many-electron systems with the electrons interacting via Coulomb and exchange interactions. The perturbation of the Coulomb potential, felt by the outer electrons when the photoelectron is emitted, causes their collapse towards a positive hole. This effect allows the possibility for the excitation of the valence electrons [92]. During the primary excitation, electrons can be to excited to higher-lying states (***shake-up process***) and the corresponding spectral lines, appearing at the higher binding energies, are called shake-up satellites. Separation of shake-up satellites in photoemission spectrum from the fully relaxed peak (primary peak) corresponds to the valence-level excitation energies concerned [93]. In the case of metals, the shake-up processes are also manifested by the existence of asymmetric core line shapes. In addition, in the case for the transition metals with ligands attached, considered within this thesis, a charge-transfer from ligand to metal (or vice versa) may occur. This leads to the occurrence of so-called ***charge-transfer satellites***, [94, 95], as first reported by

Kim and Winograd [96, 97] in 1973. Using the sudden approximation and ligand field theory they have shown that for the transition metals with a partially filled valence shell, the shake-up satellites are attributed to monopole charge transfer transitions (ligand → metal).

If the excitation happens into free continuum of states (electron is ejected rather that excited), leaving the atom in a double ionised state, the effect is called a **shake-off process** [98]. These satellites appear as a steps, followed by a continuum, instead of the satellite peaks observed for the shake-up satellites.

Due to the above considerations, the resulting spectral line-shape is a rather complex. In this thesis, I find that the combination of a pseudo-Voigt function to represent the main photoemission line together with additional pseudo-Voight functions for satellite structure provides an adequate description of the observed photoemission data.

Splitting of Core-Level Lines

In photoemission from p, d and f inner subshells the spectral lines are influenced by the coupling of the spin of the electron ($s = 1/2$) with an orbital angular momentum ($l = 0, 1, 2, 3 \ldots$ for s, p, d, f orbitals) [99, 100]. This coupling is known as **spin-orbit** or *l-s splitting.* This is a purely final state effect, since during photoionisation one electron is removed, leaving behind an unpaired spin, while in the ground state the inner subshells are completely filled. The spin can have two orientations ($m_s = \pm 1/2$), up and down, and if the orbital of the core hole has non-zero orbital momentum there will be a coupling between the unpaired electron and orbital momentum, leading to a spin-orbit doublet in the photoelectron spectrum [101]. The intensity ratio of the two spin-orbit components is dependent on the relative probability of transition to the two states, which is determined by the ratio of respective multiplicities $(2j_+ + 1)/(2j_- + 1) = (2l + 2)/2l$, where j_+ and j_- are total angular momenta for spin-up and spin-down respectively [102]. The lowest binding energy peak, corresponding to the transition to the lowest energy final state, is the one with maximum j (Fig. 2.5).
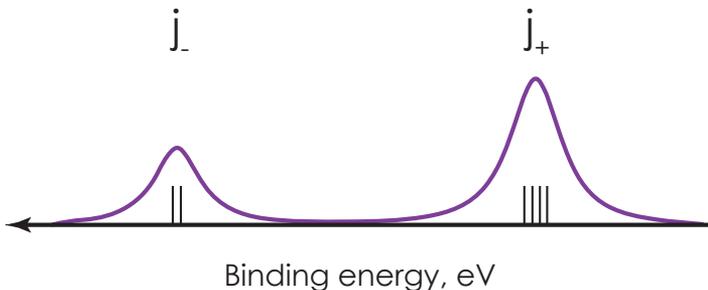

Figure 2.5: Simplified schematic representation of the spin-orbit and multiplet splitting of the photoemission signal (*p*-orbital). For a general case the amount of multiplet components m_j can be calculated as $2(2l + 1)$.

The Russell-Saunders coupling scheme described above, or l-s coupling, is sufficient to get the energies of final states, however it entirely neglects the magnetic spin-orbit interaction due to coupling between the core hole and the spin of partly filled valence levels [103]. In any atomic system, which contains unpaired valence electrons, the exchange interaction affects each spin-up and spin-down spin-orbit component unequally and favours the interaction of the core electrons with the spin parallel to the spin of the valence electrons. This nonequivalent exchange interaction leads to slight spatial displacement of the spin-up and spin-down wave functions from each other affecting the binding energies of core electrons [104]. This Zeeman-like splitting of the main lines in an effective magnetic field created by valence electrons, arranged according to the magnetic quantum number m_j, is called **_multiplet splitting_** [105, 106]. The higher the spin state of the valence electrons, the larger the splitting between m_j sublevels, broadening the photoemission lines (Fig. 2.5). This type of splitting is observed in both inorganic solids and gases, and is common for transition metals containing $3d$-series atoms [107, 108].

In addition, for transition metal complexes, the d orbitals can split in energy as a consequence of bonding to ligand orbitals. This effect occurs upon adsorption of ligands on metal surfaces or interaction of latter with metal containing compounds [99, 109]. This effect is called **_ligand field splitting_** and it can be explained within molecular orbital theory, which determines resulting molecular structure as formed by combining metal valence d orbitals with the ligand orbitals. This leads to a bigger separation between metal d levels (d_{xy}, d_{yz}, d_{xz}, d_{z^2} and $d_{x^2-y^2}$ orbitals), which is called ligand field splitting parameter or Δ parameter.

2.1.2   Theory of X-ray Absorption Spectroscopy

When the energy of the incident photon beam is equal to the difference between the electronic ground state and an excited state, photon absorption may occur. The excited state consists of an inner-shell hole, with an additional electron in a formerly unoccupied state above the Fermi level. The excited atom is typically unstable existing for core-hole life time of the order of femtoseconds, before decaying back to the ground state configuration by either radiative or non-radiative processes. Scanning the photon energy around the absorption threshold thus probes the unoccupied states of the sample through the generation of excited states and monitoring the decay characteristics. This spectral regime, close to the absorption edge threshold, corresponds to the NEXAFS (Near edge x-ray absorption fine structure) region. At energies slightly above the absorption edge threshold an additional effect plays an important role, namely the scattering of the outgoing photoelectron, which leads to the energy-dependent modulation of the photoelectron intensity in the EXAFS (Extended x-ray absorption fine structure) region due to constructive and destructive interference. The spectral lineshape in this region provides information about interatomic distances. The measurement of the absorption structure as a function of photon energy is known as X-ray absorption spectroscopy (XAS), schematic view of which is represented in Figure 2.6.

In terms of the physical principle XAS is similar to XPS. In both cases the transition is caused by absorption of a photon and excitation of an inner-shell electron, but the final states are different. In XAS the electron is excited into an unoccupied level close to the vacuum level. The final state is screened by the excited electron.

As mentioned briefly above, XAS has different names for different energy regions, due to its very broad energy spectrum. The region in the energy range from 5-10 eV below the absorption edge up to 30-50 eV above it is called X-ray Absorption Near Edge Structure (XANES) or Near Edge X-ray Absorption Fine Structure (NEXAFS). Even though that both abbreviations define in principle the same region, NEXAFS spectroscopy is typically referred for soft x-ray measurements, when XANES spectroscopy is a hard x-ray terminology [110]. For this thesis the term NEXAFS spectroscopy is applied also because it is more commonly used for K-shell absorption spectra of low-Z adsorbents on surfaces. The region from the upper boundary of NEXAFS up to a couple of hundreds of eV is called Extended X-ray Absorption Fine Structure (EXAFS) due to an extended energy range. EXAFS spectroscopy is not discussed here, considering that only the NEXAFS region is used for the work in this thesis.

Determination of the molecular orientation

Since every element has a well-defined core level structure, the position of the absorption edge provides information about the chemical species under investigation and e.g. their oxidation states. Elemental specification analysis by XAS is not used it this thesis extensively, but the remarkable advantage of XAS useful for my research is the possibility of extracting information about orientation of the adsorbate on a surface.

From molecular electronic structure it is well-known that there are two types of
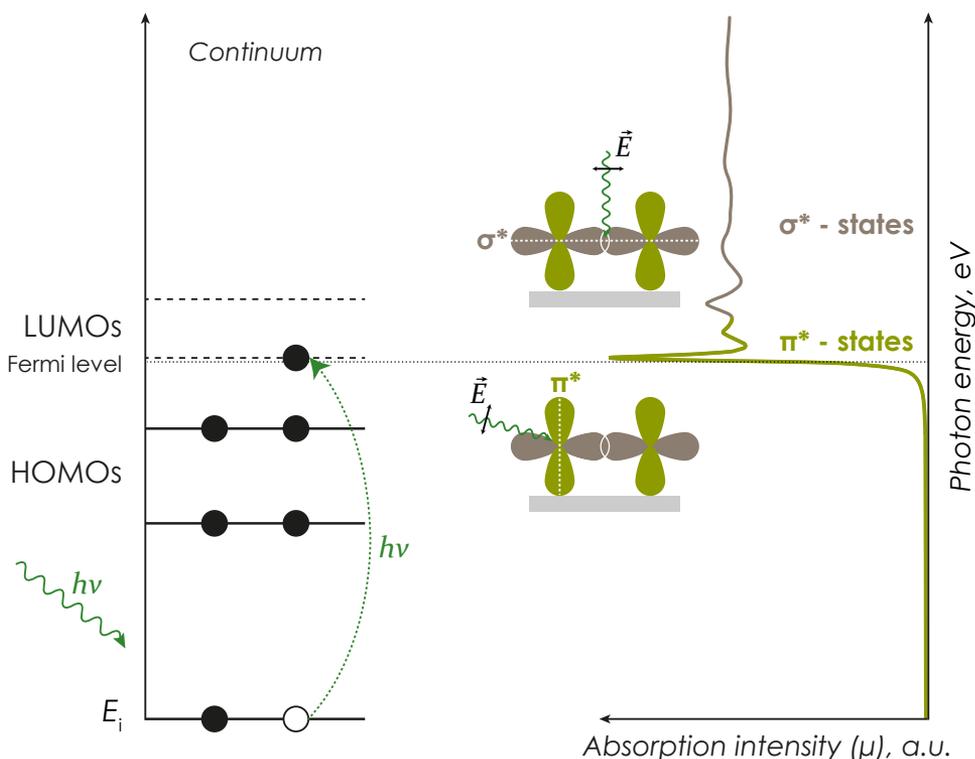
Figure 2.6: Schematic drawing of the X-ray absorption process. The left panel depicts the photoexcitation of an electron into unoccupied molecular orbitals. The right panel shows the X-ray absorption spectrum as a function of excitation photon energy. It can be divided into sharp π^* and broad σ^* resonances. In this particular case the scheme on the right-hand side shows that π^* resonances can be mapped with the electrical field vector $\vec{E}$ perpendicular to the surface, and the σ^* resonances when the $\vec{E}$ vector is parallel to the surface.

unoccupied antibonding orbitals, π^* and σ^*, which are aligned from low to high energy. A sigma resonance (σ^*) in the absorption spectrum appears due to the creation of a sigma bond. It is a covalent type of bond, typically a single bond, while a π-type bond describes a multiple bonding. The π^* resonances typically appear as the first couple of peaks in absorption spectrum and represent transitions from the core level to the lowest unoccupied levels.

Whether the resonances appear as sharp or broad features in absorption spectrum is defined by transition energy. If the transition energy of the resonance (π^* or σ^*) is below the ionisation energy, it is a trapped state and thus appears as a sharp resonance. If the transition is above the ionisation energy, the excited states appear to be less bound resulting in a shorter lifetime and broader features in absorption spectrum in higher photon energies. Thus for well-oriented on a surface molecules using linearly polarised light one can measure an absorption spectrum and by shape and position of resonance

intensities, associated it with π^* and σ^* final state orbitals, to determine the molecular orientation.

The transitions measured in XAS obey the dipole selection rule ($\Delta l = 1$), which applies that the excitation from the core level with initial state of s symmetry will take place only into unoccupied levels which have at least particial p character.

From a quantum mechanics perspective, if photoexcitation is considered to be a one-electron process, the absorption cross-section and transition rates can be defined by Fermi's Golden Rule (Eq. 2.5), as in the case of X-ray photoemission (see section 2.1.1.). The change in resonance intensity is proportional to the change of the X-ray absorption cross-section [110]

$$I \propto \frac{1}{\mid \vec{E} \mid^2} \mid \langle f \mid \vec{E} \cdot \vec{p} \mid i \rangle \mid^2 \propto \mid \langle f \mid \vec{e} \cdot \vec{p} \mid i \rangle \mid^2, \tag{2.13}$$

where $\vec{e}$ is a unit vector in the direction of light polarisation (electric field vector $\vec{E}$), and $\vec{p}$ is the momentum operator, which can be expressed using the dipole operator $e\vec{r}$: $I \propto \mid \vec{e} \langle f \mid \vec{r} \mid i \rangle \mid^2$.

The matrix element $\langle f \mid \vec{r} \mid i \rangle$ defines the direction of the final state orbital and is further described by a vector $\vec{O}$ (Fig. 2.7 inset). Assuming 100% linear polarised radiation, and a K-shell excitation, the signal intensity can be written as a function of the angle Θ between the electric field $\vec{E}$ vector and the direction of the final state orbital (Figure 2.7):

$$I \propto \mid \langle f \mid \vec{e} \cdot \vec{r} \mid i \rangle \mid^2 \propto \mid \vec{e} \cdot \vec{O} \mid^2 \propto \cos^2 \Theta. \tag{2.14}$$

According to Eq.2.14 the maximum intensity of the electron transition is obtained when the electric field vector is oriented parallel to the final state orbital (π^* or σ^* plane), as it is presented in Figure 2.6 (right panel).

In the discussion above the light is assumed to have a degree of linear polarisation of 100%, meaning one direction of the polarisation in the plane of the x-ray light oscillation. In reality, however, the degree of linear polarisation is not exactly 100% and there are two components of the electric field with different contributions ($\vec{E^{\parallel}}$ and $\vec{E^{\perp}}$). The intensities associated with these components shall be denoted as $I^{\parallel}$ and $I^{\perp}$, respectively. The intensity I can then be written as

$$I = A[PI^{\parallel} + (1 - P)I^{\perp}], \tag{2.15}$$

where A is a parameter representing the absolute resonance intensity for a specific geometry, and P is the degree of linear polarisation.

The angle Θ between the electric field vector $\vec{E}^{\parallel}$ and the vector $\vec{O}$ along a π^* or σ^* final state orbital can be defined as a function of the incident angle θ of the x-ray light and the azimuthal angle ϕ and polar angle α of the vector $\vec{O}$. For twofold and higher substrate symmetry the angular dependence of the resonance intensity for $\vec{E}^{\parallel}$ and $\vec{E}^{\perp}$
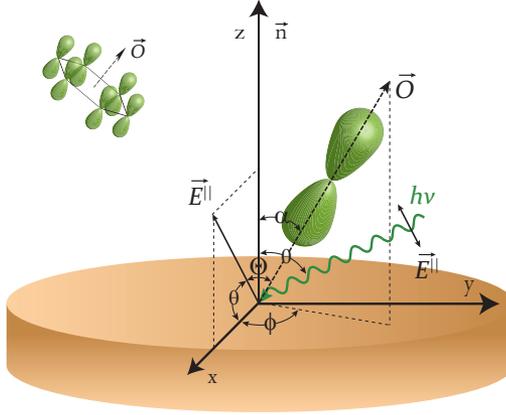
Figure 2.7: Coordinate system for determining the angular dependence of the π^* and σ^* resonances in XAS spectra. The orientation of a π^* or σ^* orbitals can be defined by the vector $\vec{O}$, that is characterised by a polar angle α and an azimuthal angle ϕ. The probing X-ray light contains the major electric field component $\vec{E}^\parallel$ and weak $\vec{E}^\perp$ component. The weak $\vec{E}^\perp$ component in this schematics is missing since the light is considered to be 100% linearly polarised. The incidence angle of x-ray light with respect to surface normal, which is also the polar angle of $\vec{E}^\parallel$, is defined as θ. For this schematics only the π^* final state orbital is presented.

components can be obtained as following

$$I_p^\parallel = 1 - \cos^2(90 - \theta)\cos^2\alpha - \sin^2(90 - \theta)\sin^2\alpha\cos^2\phi \tag{2.16}$$

and

$$I_p^\perp = 1 - \sin^2\alpha\sin^2\phi \tag{2.17}$$

According to Equation 2.15, the absolute resonance intensity dependence on the incident angle θ is obtained as

$$I_p(\theta) = A[P(1 - \cos^2(90 - \theta)\cos^2\alpha - \sin^2(90 - \theta)\sin^2\alpha\cos^2\phi)$$
$$+ (1 - P)(1 - \sin^2\alpha\sin^2\phi)]. \tag{2.18}$$

The above equation demonstrates that it is possible to determine the exact orientation of molecules on a surface by determining how the resonance intensities in the XAS spectra vary with the incident angle θ of the x-rays.

Treatment of NEXAFS Spectroscopy Data

The spectra which are measured by NEXAFS spectroscopy cannot be used directly. Instead, one needs to calibrate the photon energy and one needs to accurately normalise the spectra. Typically, the calibration of the photon energy is performed by measuring photoemission spectra of a specific core level excited by 1st and 2nd order light. This technique is based on the fact that a grating-based monochromator transmits also a small fraction of higher order photons. Considering that the 2nd order photons possess an energy twice as high as the 1st order ones, the exact photon energy can be calculated as the difference between the kinetic energies of the 2nd and the 1st order excitations:

$$\left. \begin{array}{l} E_{kin}^1 = h\nu - E_B \\ E_{kin}^2 = 2h\nu - E_B \end{array} \right\} \Rightarrow h\nu = E_{kin}^2 - E_{kin}^1 \tag{2.19}$$

The intensities of the resonances in the NEXAFS spectra are proportional to the incident X-ray intensity and therefore, all the recorded spectra must be corrected for x-ray intensity variations as a function of time and photon energy. Time-dependent variations may originate from instabilities of the electron beam in the storage ring and the electron beam lifetime, which at the facilities used in the present work reduce over time. Changes in X-ray light intensity with photon energy occur (a) due to the fact that the undulator delivers different x-ray beam intensities at different photon energies and (b) due to non-linear energy-dependent reflectivity changes of the X-ray optical system in the beam line [111]. In addition, for extracting the NEXAFS signature of monolayer concentrations of molecules on a surface, the large background contribution from a substrate has to be removed from the measured spectra. Therefore the signal from the species of interest may only be a tiny component of the recorded raw data.

Historically, several approaches have been developed for normalisation of the signal from the sample. These are either by dividing the electron yield measured on a fine gold grid in front of the experimental chamber, or by normalisation to the current recorded on a photodiode for determination of beamline transmission [112]. Other data correction procedures include the division [114] or substraction [113] of the signal obtained from the clean surface. These approaches are not equivalent and make different types of corrections.

The placement of a gold mesh directly in the optical path and simultaneous measurement of photoelectron current provide the time- and energy-dependent variation in the intensity of synchrotron radiation. The normalisation of the NEXAFS data by dividing the raw NEXAFS spectrum by the reference signal helps to remove this variation.

Normalisation by division by the clean sample spectrum does not correct for instabilities in the X-ray source, but this correction helps to resolve which of the NEXAFS features are related to surface and which to the adsorbate. Subtraction of the clean sample spectrum does not correct for instabilities in the storage ring, the transmission function of the beamline, or the detector response functions. However, this data treatment removes spectral features due to sample impurities, substrate excitations, or direct photoemission peaks from the substrate.

In the present work both the first and second correction techniques have been used depending on which one of them was more appropriate for a particular combination of sample, energy range, and detections conditions.

After removal of a background signal, the NEXAFS spectra can finally be normalised to the intensity of the step edge at about 25-30 eV above the absorption threshold (vacuum step edge) [115]. These normalisation procedures are performed so the intensity of the recorded spectra as a function of the photon energy can be directly compared for different angles of the incident light (θ). The determination of the variation of the absolute intensity of a particular resonance, as a function of angle θ, provides direct information about the orientation of the adsorbent on the surface as has already been discussed above.

2.1.3 Spectroscopy Instrumentation

X-ray Photoelectron Spectroscopy

Modern X-ray photoelecton spectroscopy instruments combine technology from a range of different fields starting from mechanical engineering and digital/analog electronics to sophisticated electron and X-ray optics, software engineering and design. X-ray photoelectron spectroscopy is a surface-sensitive technique based on the measurement of kinetic energy and number of the electrons ejected from a sample irradiated with x-rays. In this way one can measure the elemental composition of the sample. In a simplified picture, the essential components of an XPS instrument are shown in Figure 2.8.
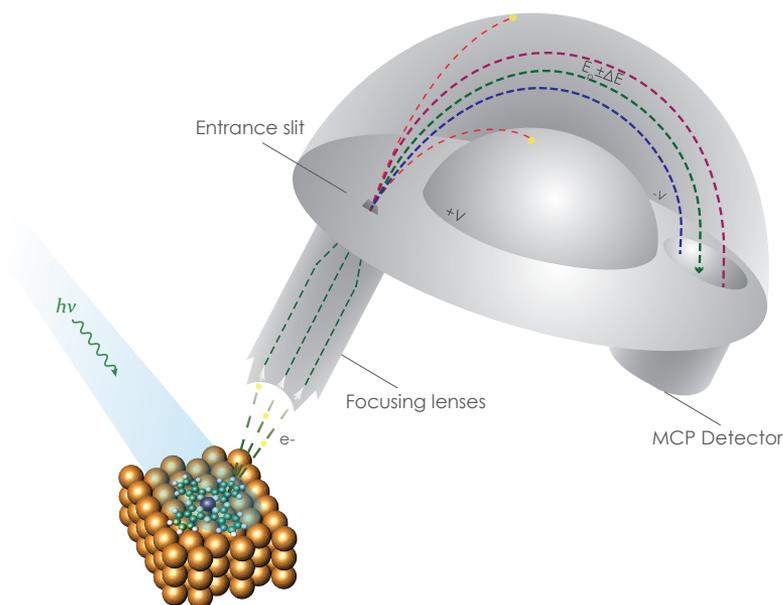
Figure 2.8: Schematic drawing of a hemispherical electron energy analyser during an XPS measurement. The photoelectrons are focused onto the entrance slit by the electrostatic lens system. Electrostatic fields within the sphere are established to only allow electrons of a given energy to arrive at the MCP detector.

The setup for XPS includes an X-ray source, an electron energy analyser and requires ultrahigh vacuum (UHV) conditions. The UHV chambers needed for both sample preparation and analysis are maintained at a base pressure in the range of $10^{-9} - 10^{-11}$ mbar to ensure that atomically clean surfaces can be prepared and maintained during the experiment and to prevent scattering of the photoelectrons between the sample and the detector. The description of vacuum systems is beyond the scope of this thesis. Detailed information about UHV technology and instrumentation can be found in references [116, 117].

Hemispherical Electron Energy Analyser

For the experimental work presented in this thesis, a hemispherical electron energy analyser such as the one depicted in Fig. 2.8 was used for measuring the kinetic energy distribution of the photoelectrons emitted by the sample. In this type of analyzer the energy selection is made by two metallic concentrical hemispheres onto which a potential difference ΔV is applied. The voltage bias forces the incoming electrons onto a curved trajectory. A specific kinetic energy is selected by the lens system that focuses the electrons onto the entrance slit and retards or accelerates them. This way only the electrons with the desired kinetic energy have the right *pass energy* that allows them to pass through the hemispheres. If the kinetic energy of the electron is too low or too high, the electron will hit the inner or the outer hemisphere, respectively. The passing electrons are dispersed through the analyser so that different energy electrons arrive at different channels of the micro-channel plate detector (MCP), where they are multiplied before reaching the fluorescent screen. Behind the fluorescent screen, a CCD camera detects the electrons as they reach the screen.

As it has been mentioned above, only the electrons with energy $E = E_{pass} \pm \Delta E$ are able to pass the analyser. The pass energy E_{pass} is set by the constant potential difference ΔV between the concentric hemispheres of the analyser. The value ΔE is the the energy bandwidth that varies with the electron kinetic energy and decreases for lower values of the pass energy. The resolution of the analyser is directly determined by the CCD as it records ΔE and divides it into channels. Thus, ΔE affects the final resolution via the number of channels and it is an important value for determining the broadening of the photoemission spectrum lines.

The electrons are travelling in the analyser along an ideal curved path with radius R_0 with some small deviation. This uncertainty together with the broadening due to the analyser entrance slit gives an additional contribution to the resolution of the analyser. The analyser entrance slit has a finite size and creates a possibility of collecting of a beam of electrons with specific angular distribution and slightly different energies, inducing additional broadening. The combination of these parameters determines the resolution of the electron analyser. This is a measure of the ability of the analyser to distinguish peaks which differ in energy by only a small amounts [118, 119]

$$\frac{E_{an}}{E_{pass}} = \frac{W_{en} + W_{ex}}{4R_0} + \frac{\alpha^2}{2}, \tag{2.20}$$

where W_{en} and W_{ex} are the widths of the analyser entrance and exit slits, R_0 is the average radius of curvature of the hemispheres and α is the angular spread of the electron beam. Both pass energy and the width of the analyser entrance slit can be changed and thus the resolution of the analyser be tuned. Both parameters also influence the intensity of the photoemission lines, and one needs to find a balance between them to achieve the most optimal result.

During my experiments, the analyser has been operated in fixed transmission mode,

also known as constant analyser energy mode. In this mode, the pass energy of the analyser is held constant and is the electrostatic lens system that lets electrons of different kinetic energies reach the detector at different times and be counted. The pass energy for fixed analyser transmission mode can be found as $E_{pass} = -ek\Delta V$, here e is the electron charge; k is a constant given for each specific hemisphere and determined by its radii; ΔV is the potential applied between hemispheres.

Light sources

The light used in photoemission spectroscopy experiments can come from several different sources, such as lasers, X-ray tubes or synchrotron radiation sources.The spectroscopy measurements described in this thesis were performed using synchrotron radiation at the MAX IV Laboratory in Lund, Sweden. The experiments were carried out at the beamlines I311 (high-resolution UHV measurements) [120] and I511 (high pressure measurements) [121], both located on the Max II 1.5 GeV storage ring. Synchrotron radiation is a polarised radiation from high energy (relativistic) charged particles, such as electrons, accelerated on a curved trajectory. Such curved trajectories are typically achieved in electron storage rings by the means of magnetic fields. The electron beam is delivered to the storage ring (MAX II) by an injector, where electrons are produced in an electron gun by thermal emission [122] and further accelerated in a linear accelerator. The electrons leave the injector in short pulses and are injected into the storage ring where the are accelerated to the final energy and further bunched together. In the storage ring the electrons circulate and are kept at speed by a radio frequency field, which the electrons pass during each turn around the ring. The radiation is emitted from the electrons in pulses in a narrow cone in the forward direction. When the acceleration is achieved by bending magnets the radiation has a broad range of photon energies.
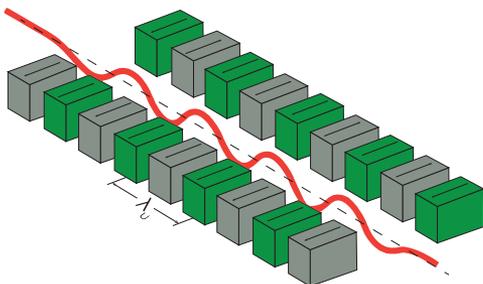
Figure 2.9: Illustration of an undulator magnet presented as a row of alternating magnets with periodicity λ_U. Image is modified from ref. [123].

To produce x-ray light and enhance the characteristics of the synchrotron radiation, insertion devices, i.e. undulators and wigglers, are placed along the straight sections of the storage ring. The insertion devices consist of periodic arrays of alternating magnetic poles that direct the electron beam onto a sinusoidal path (Fig. 2.9). Due to constructive and destructive interference of the light the electrons emit highly intense X-ray light at certain energies as well as their third, fifth, seventh, etc. overtones (harmonics). By changing the spacing between the magnetic arrays one can tune the energies of the photon

beam. High spatial brightness, i.e. flux within a small solid angle, makes undulators attractive for high-resolution spectroscopy [124]. Therefore, the work presented in this thesis has mostly been performed on undulator beam-lines, with an exception when the high flux is a disadvantage. This can be the case for some organic molecules which are prone to beam-damage from the high x-ray flux. In this case bending magnets beam-lines with lower spatial brightness have been used (beamline D1011).

Ambient Pressure X-ray Photoelectron Spectroscopy

XPS is a fundamental technique in the analysis of the elemental composition of the surfaces of materials and the electronic state of their constituents. Due to the short mean free path of electrons in the kinetic energy range up to some thousand eV, the vast majority of XPS instruments are operated under vacuum conditions and sample environment pressure does not exceed 10^{-5} mbar. However, e.g. molecular adsorbate geometries at ambient pressure can be significantly different from those observed in UHV, as a consequence of the difference in the adsorbate surface concentration and therefore, in the population of surface adsorption sites. Also, in UHV, high coverages can be obtained at cryogenic temperatures. There is a high risk, however, that the adsorbed species will be trapped kinetically and that non-equilibrium adsorbate structures are created [125, 126]. The difference between the surface reactions at ambient pressure and UHV conditions is called the *pressure gap*. For many years, this pressure gap has been an insurmountable barrier because of the large loss of photoelectron intensity owning to inelastic scattering at ambient atmosphere.
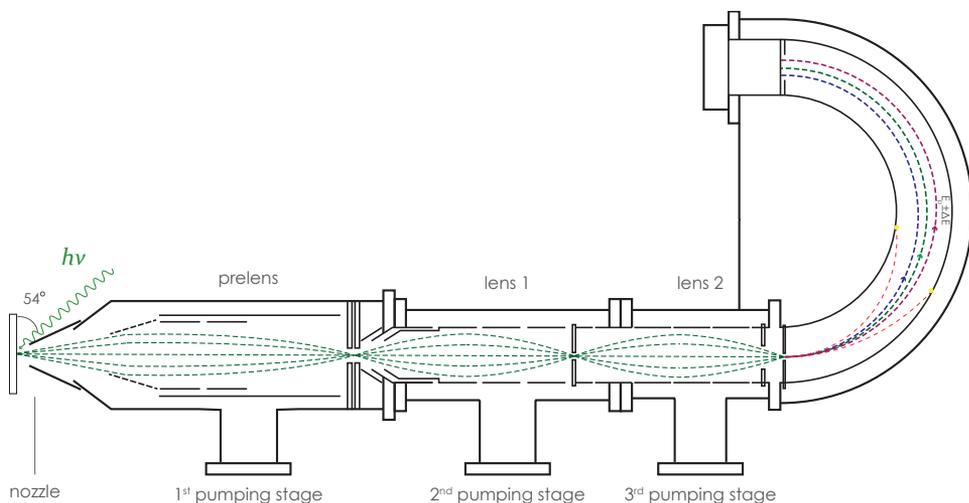

Figure 2.10: Schematic representation of electron energy analyser and pumping stages of the HP XPS setup at I511 endstation at MAX-lab. Image is modified from ref. [132].

After the first attempts to create XPS instruments for surfaces in a vapour atmosphere by Siegbahn and Siegbahn in early 70s [127, 128] and further instrument improvements

by Joyner and co-workers [129] the field of ambient pressure XPS developed continuously. The technique came to fruition with the advent of third-generation synchrotron radiation sources, due the large gain in photon flux. This helped to overcome the problem of photoelectron intensity loss due to inelastic scattering on gas molecules. Another important development was the use of electrostatic focusing in the differentially pumped lens system of the ambient pressure electron energy analysers [121,130,131]. The ambient pressure XPS measurements for this thesis have been performed at beam-line I511 at MAX IV Laboratory. The schematic drawing of the ambient pressure electron energy analyser with three differential pumping stages is depicted in Fig. 2.10. The sample is placed in a high pressure cell with gas in the analysis chamber. The sample is then moved close to a gas nozzle, at a distance typically twice the diameter of the nozzle aperture, i.e. in the range between 0.1 to 1 mm. The photoemitted electrons from the sample arrive at the first pumping stage with a prelens system, before passing on to the analyser. The lens system (prelens) focuses the electrons in a 2 mm aperture, after which the electron beam passes through two more evacuated stations in which it is being focused by lens systems (lens 1 and 2), before reaching the hemispherical analyser. The role of the pumping stations is to ensure that the pressure at the detector does not become higher than 10^{-8} mbar. In this type of setup, the pressure at the sample can reach up to 100 mbar, however a pressure of 1 mbar is most commonly used.

Temperature Dependent X-ray Photoelectron Spectroscopy

Temperature Dependent (TD)-XPS measurements were performed on molecules adsorbed on a metal surface, by gradual annealing of the sample up to 350-500°C either in UHV or ambient pressure. XP spectra were recorded for a discrete set of temperatures. As the intensity of the XPS peaks is proportional to the amount of different species on the surface, TD-XP spectra could be used for the determination of the desorption temperature (cf. Fig. 2.11). From the binding energy shifts one can identify temperature-induced surface reactions.
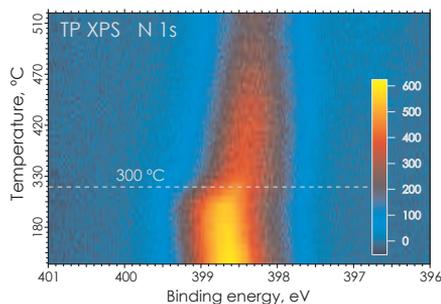
Figure 2.11: TD XPS experiment performed for a FePc monolayer. The sample has been gradually annealed to about 500°C. The color scale represents the intensity scale, indicating the desorption of the molecules from the surface.

Fig. 2.11 illustrates the temperature-induced chemical modification of FePc on a Cu(111) surface at monolayer coverage. Up to 300°C no desorption is observed. At 300°C both desorption and chemical modification of adsorbates occurs [133].

Acquisition and monitoring of X-ray absorption spectra

In the first half of this chapter the principles of X-ray absorption spectroscopy have been discussed. Now I will concentrate on the acquisition and treatment of the data. The two most convenient techniques for the measurement of X-ray absorption signal are the fluorescence yield and the electron yield methods.
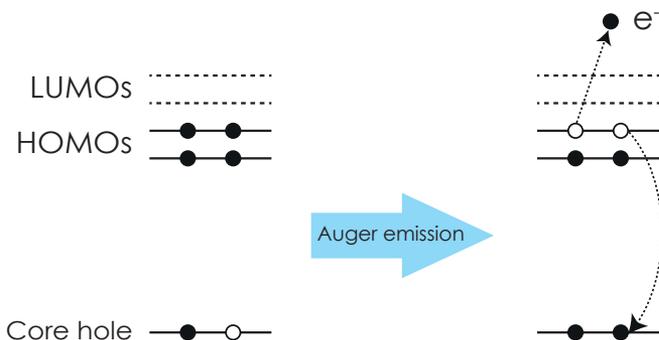

Figure 2.12: Schematic drawing of the excited-state decay upon the creation of a core hole. The hole is filled by electron from a higher shell by Auger electron emission.

The fluorescence yield method is a radiative method based on the decay of the core hole created in the X-ray absorption process. The cross section for fluorescence decay is very low for the low-Z elements such as Carbon, Nitrogen, and Oxygen. Thus it has not been employed in this work. Instead, the non-radiative decay in the form of Auger electron emission has been used, which involves filling the core hole with an outer-shell electron and releasing an Auger electron from a higher energy level (Fig. 2.12). The kinetic energy of the emitted electron is element-specific and is tightly related to binding energies. The Auger peaks can be distinguished quite easily since they are constant in kinetic energy, and the recorded intensity directly gives the X-ray absorption cross section of the specific shell of the adsorbate atom [110].

If during X-ray absorption experiment both elastically and inelastically scattered electrons are recorded as a drain current from the sample, the technique is called the Total Electron Yield (TEY). Since it detects electrons of all energies including the inelastically scattered ones from deeper inside of the sample, the TEY is a bulk sensitive method. To make it more surface sensitive, one needs to apply a certain retarding voltage to cut off the slowest electrons. This way the electron energy analyser may be used to select electrons of a particular kinetic energy and separate between photo and Auger electrons. This method is called Partial Electron Yield (PEY). Another way of detection is the so-called Auger Electron Yield (AEY). AEY requires an electron energy analyser as a detector, and only the Auger peak of interest is measured. One selects a window around the kinetic energy of the Auger peak and records the intensity of the Auger spectra over a specific photon energy region. Typically this region is chosen around the absorption edge. The measurements used in this work were performed by using both PEY and AEY techniques.

2.2 Scanning Tunnelling Microscopy

To fully characterise a surface process, it is advantageous if averaging techniques such as XP and XA spectroscopy are complemented by a local probe technique. Scanning tunnelling microscopy (STM) is an excellent tool for this purpose. It provides direct real space images of a surface of a conductive sample on the atomic scale.

After its invention by Gerd Binning and Heinrich Rohrer, who were awarded the Nobel Price for their discovery [135, 136] in 1986, the technique has rapidly became a standard surface imaging technique. The technique can provide high-resolution images with spatial resolution of approximately 1 Å in the surface plane, and 0.1 Å in the perpendicular to the surface direction [137]. In addition, STM can also provide images of large surface areas in a short time with the lowest acquisition time recorded of ∼15 msec/image [138, 139], which makes this technique suitable for time-dependent studies, e.g. dynamic phenomena. Although, the acquisition time in the order of minutes is typically used.

2.2.1 The concept of tunnelling

The principle of STM is fairly straightforward, employing an atomically clean and sharp tip, which is brought to within a fraction of a nanometer distance to a conductive surface. The electron wave functions of the surface overlap with those of the tip, and by applying a small potential difference a finite tunnel current is generated. Typically, the bias V is specified in terms of the voltage applied to the sample [140]. This means, that if the sample is biased positively ($V > 0$), an energetic incentive is provided for electrons to tunnel from the occupied states of the tip into unoccupied states of the sample. When $V < 0$, the electrons tunnel from the sample into the empty states of the tip. The tunnel current depends exponentially on the distance between the tip and surface, so the larger the distance, the smaller the current. Thus, by measuring the fluctuations of the tunnel current as the tip is scanned across the surface, a topographic image is recorded.

In simplified picture, an electron in a potential well is considered as a ball trying to roll over the hill. Classical mechanics scenario predicts that the ball cannot pass trough the wall. In contrast, in quantum mechanics the electron has a small, but non-zero probability of going through (tunnelling) the wall - or the potential barrier. The reason for this dissimilarity originates from the fact that matter has both waves and particle character. Thus, according to Heisenberg's uncertainty principle, which defines a limit of precision of either the location or the velocity of the particle at the same time, there are no solutions with a probability of exactly zero. Hence, the probability of the particle's existence on the other side of the potential barrier is non-zero [141].

If two metals A and B are brought to within tunnelling distance of each other, with metal A biased relative to B by a voltage V, the Fermi levels are offset from their equilibrium position (Fig. 2.13). This equilibrium position is originally obtained through rapid charge transfer when metals are brought together. The applied bias offsets the Fermi energies on one side of the vacuum barrier and this creates a potential difference, which further establishes a net tunnelling current between the metals A and B. The
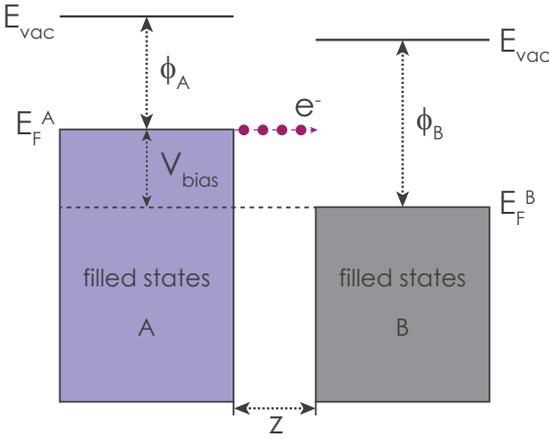
Figure 2.13: Energy levels of two metal electrodes, A and B, during vacuum tunnelling. Positive bias is applied to metal B, so electrons tunnel from the metal A to B ($V_A < 0$). Image is inspired by [142].

tunnelling current between the metals depends strongly on the separation z between two solids and in simple planar tunnelling model using the Wentzel-Kramers-Briullouin (WKB) approximation, it is given by

$$I = \rho_A \rho_B V_A exp(-2\sqrt{m(\phi_A + \phi_B)/\hbar^2}z), \qquad (2.21)$$

where ρ_A and ρ_B denote the local density of states at the two solids, V_A is the applied bias, m is the mass of the electron, ϕ_A and ϕ_B are the work functions of surface of A and B, respectively, and z is their separation [143]. The strong dependence of the tunnelling current on the separation is the origin of the high resolution in the STM probe, which is typically below 1/100 monolayer for most solid surfaces.

Equation 2.21 also reveals that STM images display not purely topographic changes on the surface, but rather a complex mixture of electronic and geometric features. Therefore, with the tip-surface separation too big to create a chemical bond, either the atomic relaxation or a local charge density can change during the scanning process, which affects the value of the tunnelling current and gives rise to an apparent height difference. Note, that the absolute height of the adsorbent species on the surface cannot be accurately determined with STM. Qualitatively, atoms with higher chemical affinity have a higher tunnelling conductance and are imaged at a larger apparent height [143] than they are in reality.

2.2.2 Instrumentation

A schematic diagram of a typical STM setup is illustrated in Figure 2.14. The figure contains the most important components, which include a scanning tip, piezoelectric controlled height, and xy scanner and a conductive sample [144]. The atomically clean and sharp tip is attached to a 3D piezoelectric scanner. By adjusting the piezovoltage, the position of the tip can be precisely controlled since a piezoelectric material is mechanically deformed when an electric field is applied. The tip is scanned in the surface

plane by independent piezo elements in the x and y directions and a piezo element in z direction controls the lateral position.

There are two common STM operation modes, the constant current and constant height modes. In constant current STM imaging the tip is moved across the surface and a constant tunnel current is maintained during scanning. Imaging is done by vertically moving the tip at each data point until the setpoint current is reached. The vertical position is stored and used to form the topographic image of the sample surface. This method is the most commonly used in STM.

In the constant height approach the tip-sample distance is kept fixed and a variation in tunnel current forms the STM image as a current map, $I(x, y)$. This current map represents a cut through charge density contours in the plane chosen by tip height. This approach allows higher scan speeds because no feedback signal is necessary. However this technique can only be used for flat samples with zero curvature of the surface.
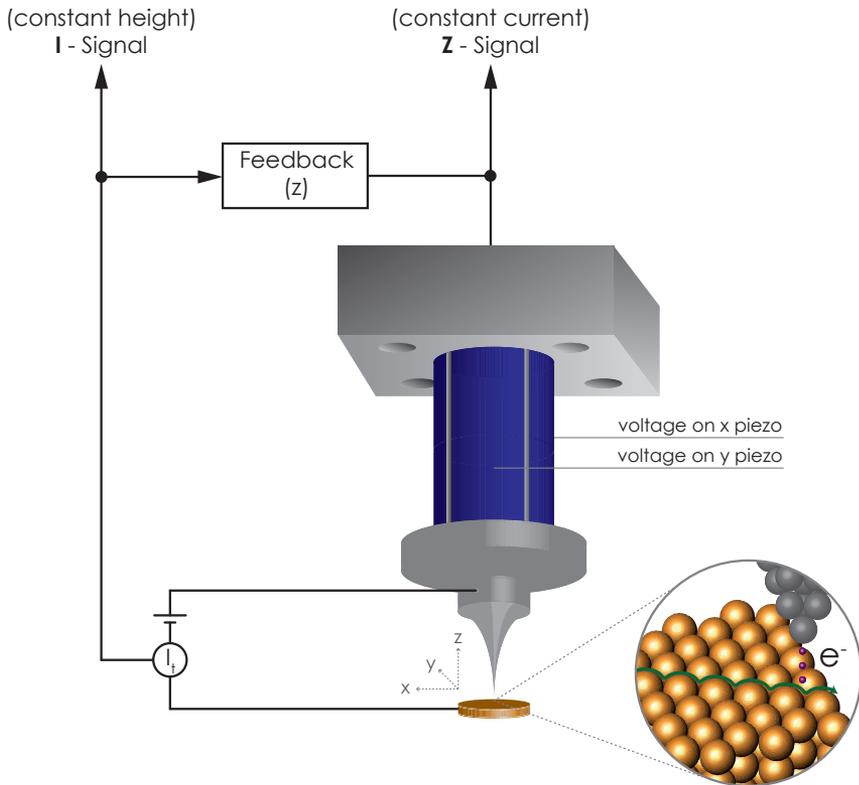
Figure 2.14: Schematic illustration of the various components of a scanning tunnelling microscope system. The tip probes the surface by scanning in x- and y- directions by use of piezoelectric tube scanner for positioning the STM tip. The tunnelling current or the tip-sample distance is set by user. In the case of constant current mode, the feedback loop helps to continuously adjust the position of the tip while scanning in such a way to maintain the tunnelling current constant.

Since the probe tip is only a distance of order of 1 nm away from the surface, any mechanical vibrations of the tip relative to the sample have to be minimised to the picometer scale. This low vibration is achieved by the microscope being constructed in the way that the sample and the tip are placed on a rigid platform, which is hold on springs or dampers inside the SMT chamber. In addition, the entire microscope is mechanically isolated from any vibrational sources by placing it on mechanical springs or gas damping systems [140].

CHAPTER 3

Results

The following chapter provides a summary which highlights the most interesting points of the results from the papers that are included in this thesis. The aim of this chapter is to present the relationship in motivation between the separate publications and manuscripts.

Surface modifications of iron phthalocyanine on Cu(111)

Since the discovery of iron phthalocyanine its interaction with different types of ligands has been investigated extensively [18–23]. These studies have shown that the electronic configuration of the molecule and specifically of its iron centre can be manipulated by adsorption of different ligands on top of the compound. These results have led to the conclusion that the quantum properties, such as the compound's spin state, arising from the unpaired electrons in the valence shell of the iron atom, can be tuned to a desired value by ligand adsorption. This realisation of this tuning of the electronic states in phthalocyanine, via the interaction with small ligands, has led to the idea of tuning the molecular electronic states by choice of the surface material. This would allow the modification of the electronic configuration in a way identical to that of ligand adsorption, but from beneath the molecule. This, in turn, would then allow the molecule's electronic properties to be further tuned by varying the ligand species.

To date, many research groups interested in surface-driven changes in the electronic structure of iron phthalocyanine have investigated the adsorption of FePc compound on various surfaces [25, 145–152]. These works have demonstrated explicitly that the molecule-surface interaction leads not only to the possibility of spin state manipulation [25], but also that it alters the symmetry of the molecule [34], which in the gas phase exhibits a perfect fourfold symmetry (Fig. 1.1).

Indeed, when adsorbed on moderately reactive or non-reactive surfaces, such as Au(111) or HOPG (highly oriented pyrolitic graphite), FePc appears with a fourfold symmetry in STM images, at both monolayer and sub-monolayer coverages [147–149]. However, when the molecules are deposited on more reactive transition metal [31, 32] or on insulator surfaces [53], it has been reported that the symmetry of the compound changes from C_{4v} to C_2, for adsorption up to sub-monolayer coverage. This phenomenon of lowering of the original C_{4v} symmetry to C_4, C_2 or C_1 will be further referred as a *symmetry reduction* or symmetry breaking.

The symmetry breaking of FePc molecules on the Cu(111) surface, was first reported by Chang et al. and this effect was attributed to the distortion of the molecule's macrocycle [34]. However, these conclusions have been somewhat controversial. While some STM groups claim that the symmetry breaking of MPcs is purely geometric in origin (topographic) [37, 40], other groups argue that it is either purely electronic [32] or that it is a geometry-driven electronic effect [31, 34, 35, 41]. Currently, there exists no consensus as to the origin of the observed symmetry breaking in the surface science community, and one of the aims of this thesis is directed towards resolving this issue by combined imaging and spectroscopy approaches.

As discussed in Section 2.2, one of the drawbacks of STM is that it does not provide purely topographic information but rather a complex convolution of geometric and electronic properties. Therefore, it is difficult to fully explain the observed symmetry breaking of adsorbed metal phthalocyanine molecules and to ascribe it to one of the possible origins by only considering STM data. One of the techniques that can provide information on charge transfer effects is XPS [153], in particular when supported by theoretical calculations. Therefore, in the work with the present thesis, photoelectron spectroscopy measurements were performed to achieve a full characterisation of the adsorption of the FePc molecule on different surfaces and these data were combined with theory to quantify the geometric and electronic contributions to a symmetry reduction.

Orientation of Fe phthalocyanine on Cu(111)

At submonolayer coverage FePc adsorbs on the Cu(111) surface with the iron ion in a bridge site [134, 150] and with one of the molecular axes in perfect alignment with one of the equivalent crystallographic directions of the sixfold symmetric Cu(111) surface. Here, a molecular axis is defined as one of two dihedral axes aligned parallel to opposite isoindole units of the molecule's macrocycle (marked green and purple in Fig. 3.1).
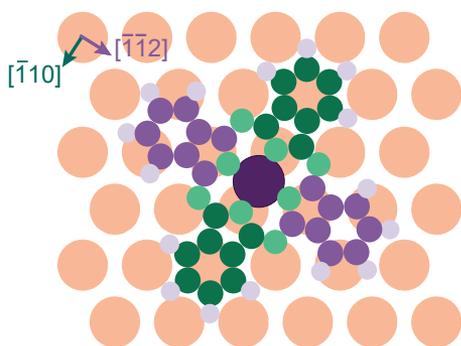
Figure 3.1: Schematic representation of a single FePc molecule adsorbed on Cu(111). The representation corresponds to orientation of FePc observed in STM with the iron ion in a bridge adsorption site and one of the molecular axis aligned with one of the close-packed crystallographic direction of the Cu(111) surface ($[\bar{1}10]$) [134]. The axis aligned with the $[\bar{1}10]$ crystallographic direction is marked green, and the perpendicular one in the $[\bar{1}\bar{1}2]$ direction is marked purple.

By means of DFT calculations, the optimised structure of FePc on Cu(111) shows the distortion of the macrocycle of the molecule (**Paper I**) and as a result, the bending of the axis aligned in $[\bar{1}\bar{1}2]$ direction $\sim$0.2 Å down to the surface.

X-ray photoelectron spectroscopy characterisation of FePc on Cu(111) in combination with the first principles calculations

The FePc molecule can be fully characterised by analyzing the C 1s, N 1s and Fe 2p XP photoemission spectra. Before discussing the analysis of surface-induced modifications of FePc adsorbates, we first assign the carbon and nitrogen species of pristine FePc molecule. Multilayers of FePc have been studied previously on inert surfaces, such as HOPG (Fig. 3.2 (b)). Due to both the weak substrate-adsorbate interactions at this surface and due to the weak intermolecular interactions, the absorption process does not change the chemical and electronic states of the molecules significantly [18], and the multilayer can be considered a reliable model of the pristine FePc molecule.
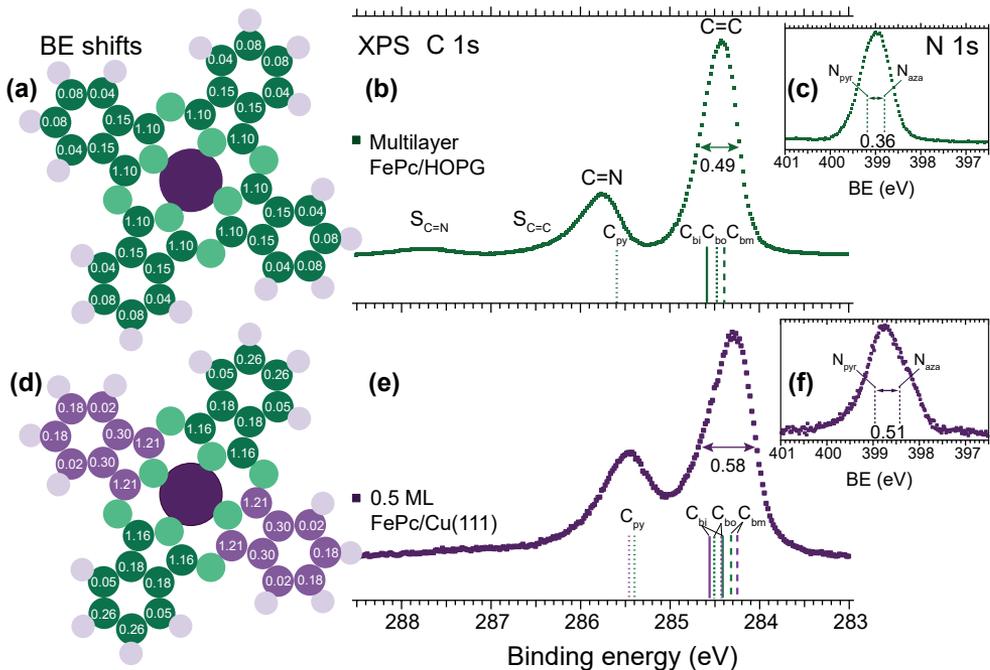
Figure 3.2: Experimental and theoretical C 1s and N 1s XP spectra of a thick multilayer of FePc deposited on HOPG, representing the properties of pristine FePc, and for 0.5 ML FePc adsorbed on Cu(111). (a) and (d) Calculated binding energy shifts. (b and e) The C 1s photoemission lines consists of contributions from the C=C, C=N, S$_{C=C}$ and S$_{C=N}$ components. (c and f) experimentally recorded N 1s XP spectra.

For the FePc in multilayer on HOPG surface the C 1s XP spectrum consists of two main components (Fig. 3.2 (b)). The most intense feature at around 284.5 eV results from the photoemission of C 1s core level electrons from the 24 carbon atoms of the benzo groups (labelled C=C). The second feature, at higher binding energy (285.85 eV),

is due to the contribution from the eight pyrrole carbon atoms (labelled C=N) that are bonded to pyrrole nitrogen atoms. Both of the main core level photoemission lines are accompanied by shake-up satellite structures shifted by approximately 1.8 - 2 eV to higher binding energy ($S_{C=C}$ and $S_{C=N}$) [154–156].

The full width at half maximum (FWHM) of the C=C peak contains information about the chemical shifts of the different carbon atoms of the benzo group. The carbon atoms in the benzo moiety of the FePc molecule have different chemical environments, which results in three different carbon contributions to the C=C photoemission peak: C_{bo} (outer), C_{bm} (middle) and C_{bi} (inner) (Fig. 3.2 and Fig. 1.1). The FWHM of C=C peak for FePc/HOPG includes all of these contributions (0.49 eV) in addition to all lineshape broadening mechanisms discussed in section 2.1.1. If the conditions of the experiment are not changed, the contributions to the FWHM due to instrumental broadening stay constant and the phonon broadening is not expected to change significantly. Therefore, any additional line-shape broadening after adsorption of the molecule on a different surface is caused by surface-induced chemical shifts with both initial and final state effects. The FWHM of the pyrrole carbon (C=N) peak is not discussed here as it contains a $S_{C=C}$ shake-up satellite contribution, the intensity of which can vary with the strength of the adsorbate bonding to the surface.

The N 1s XP spectrum of a FePc multilayer on HOPG consists of one characteristic photoemission line (Fig. 3.2 (c)). Despite the fact that the FePc molecule contains two chemically inequivalent nitrogen species, the pyrrole nitrogen atoms (N_{pyr}) and nitrogen that bridges together the isoindole parts of the molecule (N_{aza}), the binding energy peaks for these two components are separated by only 0.36 eV and cannot be resolved experimentally.

The line of the C 1s and N 1s core level spectra of the FePc multilayer are symmetric; upon deposition of submonolayer or monolayers of FePc onto the clean Cu(111) surface, however, the N 1s and C 1s core level lines get broader and obtain some degree of asymmetry. This is a clear evidence that the surface has a strong impact on the properties of the adsorbed molecules. The FWHM of the peaks at submonolayer is broadened by $\sim$ 0.1 eV, which indicates surface-induced chemical shifts for the benzo moieties of the molecule. The separation between the C=C and C=N photoemission peaks is also significantly reduced from 1.33 to 1.2 eV.

In **Paper I**, the ultraviolet photoelectron (UP) spectrum of FePc on Cu(111) shows clear evidence of a charge transfer between the molecule and the surface. It is visible from the occurrence of a new feature at 0.6 eV binding energy, which has been assigned to a formerly unoccupied molecular orbital. This is indicative of a charge intake from the surface into the molecular orbitals. These results are consistent with a scenario in which the properties of the FePc molecule are modified by the charge transfer from the surface. Therefore, the combined ultraviolet photoelectron spectroscopy (UPS) and XPS results, together with density functional theory (DFT) calculations of binding energy shifts and a Bader charge transfer analysis, provide powerful insight into the nature of the symmetry reduction mechanisms in FePc adsorbed on a Cu(111) surface.

The calculations of the intake of the electron density by the molecule from the surface, as analysed in a Bader charge analysis, show the transfer of almost one electron, which is unequally redistributed over the macrocycle of the molecule. The calculations show
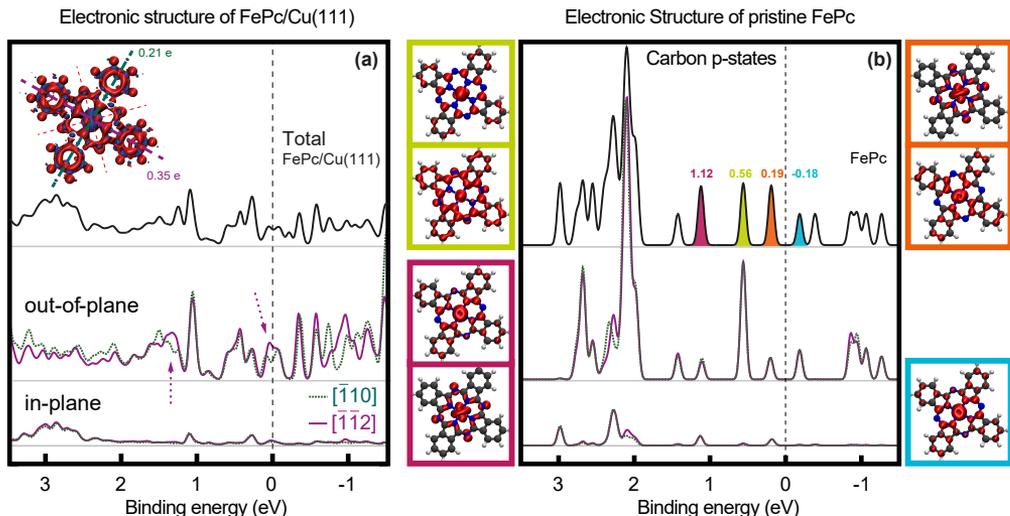
Figure 3.3: Carbon pDOS of the *p*-states of (a) FePc adsorbed on Cu(111) and (b) the free FePc molecule. For FePc on Cu(111) the total *p*-pDOS is separated into the contributions along the different molecular axes.

that the majority of the electron density is transferred to the molecular axis with the orientation perpendicular to the close-packed direction of the surface ($[\bar{1}\bar{1}2]$), while only a minor part is transferred to the molecular axis aligned with close-packed Cu(111) crystallographic direction ($[\bar{1}10]$) (inset in Fig.3.3 (a)).

The calculated partial density of carbon *p*-states (*p*-pDOS) of FePc on Cu(111) shows a clear difference to that of the free FePc molecule (Fig. 3.3). The out-of-plane contributions along different FePc axes confirm that the *p*-states of the FePc carbon atoms on the molecular axis that are aligned with $[\bar{1}\bar{1}2]$ direction of the surface has the most significant contribution close to the Fermi edge. This observation is accompanied by the fact that this axis bends towards the surface. Having determined this fact, the next question is whether it is the charge intake that bends the axis towards the surface, or whether the bending causes the higher charge intake? The cause-consequence relation between these two effects cannot be resolved from these results. However, irrespective of which of these effects comes first, the different charge intake on different molecular axes is mirrored by core-level photoelectron spectroscopy data, and in my work I show this for the first time.

The comparison of the binding energy shifts of the C 1*s* and N 1*s* core levels of FePc in a thick multilayer on HOPG and at submonolayer coverage on Cu(111) show that on copper surface the binding energies for atoms in both pyrrole rings and benzo moieties on different molecular axes are significantly different (Fig. 3.2 (d-f)). This results in an increased FWHM and asymmetry of the C 1*s* and N 1*s* lines of FePc/Cu(111). Thus, my research shows that the symmetry breaking is observable not only in STM images, but it is also evident from the change in lineshape of the core level photoemission lines.

To address the question of whether the binding energy shifts in the broken-symmetry sample are due to electronic effects or due to the surface-induced distortion of the macrocycle of the molecule, the binding energy shifts have been separated into 'distortion' and 'surface' contributions (**Paper I**). By 'surface' contribution I imply the contribution induced by the presence of the surface, e.g. charge transfer and core hole screening effects. By the absolute values of the contributions, it is clear that the 'surface' contribution has a bigger impact; this result suggests, however, that both contributions influence the binding energy shifts significantly. This means that the nature of the symmetry reduction is a rather complex combination of both the electronic and structural effects.

In **Paper II** I have shown that the symmetry breaking occurs for different coverages and is a coverage dependent effect. Symmetry reduction occurs for singly adsorbed molecules and up to a coverage of one monolayer. The molecules in the overlayers above the first molecular layer are electronically decoupled and show no sign of charge transfer from the surface. This is evident not only from the absence of symmetry breaking in STM images, but also in the XP spectra. The XPS data shows that the second layer of the FePc molecules appear as a new contribution shifted by 0.45 eV towards higher binding energy.
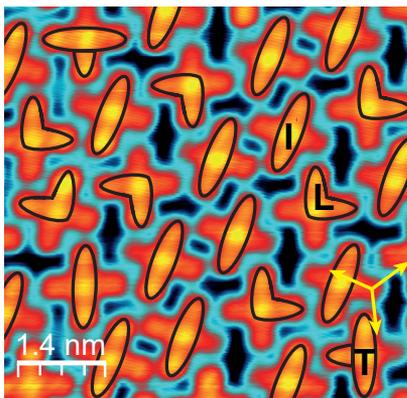

Figure 3.4: STM image of an FePc/Cu(111) assembly at monolayer coverage. The colour scale of the image is chosen to illustrate clearly the different types of symmetry reduction (I, T and L-types). In addition, also fully symmetric molecules can be observed (not shown). For the I-type of adsorbate the bright axis deviates by $90°$ from the dense-packed Cu direction.

For different submonolayer coverages (up to 0.65 ML) symmetry reduction can lead to molecules which appear with bright axis along different surface directions, aligned either with $[\bar{1}10]$ or $[\bar{1}\bar{1}2]$ the crystallographic direction of the surface, but it always remains of twofold symmetry. Interestingly, for a higher coverage of around one monolayer, I have observed different types of onefold symmetry with only few molecules remaining with twofold symmetry (Fig. 3.4). This is a clear indication that, upon the creation of the monolayer, the FePc molecules change the adsorption site on the surface, which results in a different charge redistribution together with different distortions of the molecules' macrocycle.

Temperature–induced modification of FePc on Cu(111)

The heating of the sample to the evaporation temperature of the adsorbate is a widely used technique for the creation of a molecular monolayer [18, 48, 149, 157]. By increasing the temperature, i.e. annealing, of the sample one can easily remove most of the weakly bonded species from the surface, including the molecular adlayers. The second and further layers of the molecules on a surface are typically more weakly bonded to the surface than the first molecular layer, and by adjusting the sample temperature one can remove the required amount of adsorbates from the surface. This technique is the simplest way to achieve a single molecular layer since it does not require any additional sophisticated and expensive equipment to ensure a proper molecular coverage. Therefore, this approach is a favoured method for a large scale industrial applications, such as creation of molecule-based devices.

Despite the simplicity of the method, annealing technique has its drawbacks. In recent years, a number of publications have reported that the temperature treatment of the surface can modify the properties of the molecules adsorbed on this surface. The modifications are rather mild in some cases, such as the reorganisation of the molecules and the creation of more closely packed layers of the adsorbate on a surface [158]. However, more drastic effects can also occur in other cases, such as temperature-induced chemical reactions. For some supported organic compounds, such as porphyrins and phthalocyanines, it has been shown that the annealing can cause dehydrogenation of the molecules leading to a homocoupling reaction [159, 160]. In the homocoupling reaction, the molecule looses some of its hydrogen atoms and neighbouring molecules merge together. The temperature-induced homocoupling is shown to take place only for the molecules that are adsorbed on more reactive transition metal surfaces, such as copper or silver, while it does not occur for phthalocyanine molecules on the less reactive surfaces, such as gold [18, 19].

In **Paper II** I have examined the changes of the geometric and electronic structure of the FePc molecules adsorbed on Cu(111) induced by thermal annealing by combining imaging (STM) and spectroscopy (XPS, XAS) techniques. The motivation for the rather extensive study is the observatiion of significant broadening of the C=C peak in the C 1s XP spectrum after annealing of the sample at temperatures between 250 and 320°C (Fig. 3.5). The position of the C=C peak remains rather unchanged, while a broadening towards both low and high binding energy is found. This can be explained by the presence of at least two new components in the C 1s XP spectrum.

To fully understand the origin of the new components in the C 1s XP spectrum, STM has been used. The analysis of the STM images before and after annealing of the FePc molecules on Cu(111) at different coverages reveals that despite the temperature-induced rotation of some single adsorbed FePc molecules the symmetry reduction is still pronounced. This indicates that the symmetry breaking still contributes to the FWHM of the benzo carbon atoms peak. Additionally, STM data show that annealing of the FePc molecules leads to a homocoupling reaction, caused by the removal of some of the hydrogen atoms from benzo moieties and subsequent reaction with neighbouring molecules. Therefore, some of the C-H bonds in the annealed FePc molecules are replaced
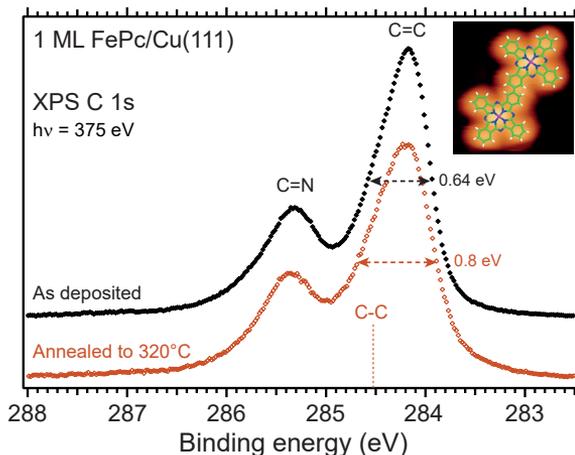
Figure 3.5: C 1s XP spectra recorded for 1 ML coverage of FePc on Cu(111) before (black) and after annealing to 320°C (orange spectrum). Both spectra have been recorded at room temperature. The full width at half maximum of the benzo peak of the annealed FePc molecules comparing to that of the FePc before annealing has increased from 0.64 to 0.8 eV. Inset: STM image of FePc/Cu(111) after annealing and its schematic model show homocoupling reaction.

by C-C bonds, which leads to a C 1s binding energy in the involved carbon atoms that is around 0.20 to 0.36 eV higher than that of the other benzo carbon atoms [161]. This may also explain the broadening of the benzo peak to the high binding energy side in the C 1s spectrum.

The broadening of the benzo peak on the low-binding energy site can be explained by the reduced distance between the surface and the adsorbate. In the discussion part of **Paper II** I support this assumption by the observed binding energy shifts of N 1s and Fe 2p XP spectra towards lower binding energy. The downshifts are likely to appear from a stronger surface-adsorbate interaction, since a closer distance would lead to a more efficient core hole screening.

The possibility of occurrence of this low binding energy component due to the temperature-induced breaking of some molecules on the surface is not considered, as there has been no indication in the STM images of such dissociation taking place. The other possibility of such a downshift could be an increased charge transfer from the surface as a result of annealing. However, the π^* lineshape in the N 1s XA spectra remain unchanged and since the intensity contributions of the resonances are directly linked to the occupation of the unoccupied molecular orbitals probed in XAS, these results do not support the possibility of an additional charge transfer from the surface.

The shortened surface-adsorbate distance upon annealing indicates that the annealing leads to a weakening of the intermolecular bonds, breaking of some π-type bonds and their switch-over to σ-type bonding to the surface. Further support, in addition to that from XAS and XPS, come from the observation that the annealed FePc molecules on Cu(111) exposed to atomic oxygen experience molecular decomposition, while it is not the case for the room temperature prepared FePc monolayer. This effect, also known as

the second chemisorptive state, have been shown to occur previously only for smaller molecules adsorbed on transition metal surfaces [162]. However, in **Paper II** I have demonstrated this to also occur for the supported phthalocyanine molecules for the first time.

FePc on copper nitride: link between geometry and spin state

As discussed previously, the nature of a support can dramatically influence the structural and electronic properties of an adsorbate. In the case of the Cu(111) surface, the surface-induced modifications are clearly triggered by the reactivity of copper and the arrangement of the surface atoms. Therefore, the creation of a single layer of copper nitride on a Cu(111) surface would be expected to decouple the molecules from the surface and remove most, if not all, surface-induced effects. This expectation is based on previous studies, which have demonstrated that the nitride overlayer has isolating properties and is inert to many ligands [163, 164].

Self–organisation of adsorbed atomic nitrogen on the reconstructed Cu(111) surface

Copper surfaces do not dissociate molecular nitrogen, so the surface atomic nitrogen chemisorption phase on the Cu(111) surface was prepared by a low energy nitrogen ion bombardment. Previous studies show that atomic nitrogen adsorption on the Cu(111) surface leads to reconstruction of the outermost layer. This reconstruction is believed to be related to the relief of surface stress and results in the outermost layer with the pseudo-Cu(100)$c(2\times2)$-2N surface phase [163–166]. The surface nitrogen atoms in this reconstructed layer occupy fourfold hollow sites as presented in the Fig. 3.6. The unit cell of this structure is face-centred $c(2\times2)$ with two nitrogen atoms, i.e. $c(2\times2)$-2N.
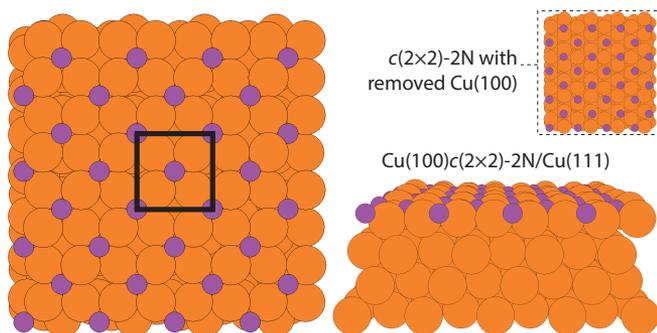

Figure 3.6: Top and side views of Cu(100)$c(2\times2)$-2N created by atomic nitrogen adsorption on Cu(111) which caused the reconstruction of the outermost layer. The structure is identified in the DFT calculations. Nitrogen atoms are marked by purple colour circles, and copper - by orange. Square structure defines the unit cell of $c(2\times2)$ structure.

The pseudo-(100) reconstruction of Cu(111) affects only a single atomic layer and the second layer of copper keeps its sixfold crystallographic symmetry [167]. This means that Cu(100)c(2×2)-2N created on Cu(100) a surface can have different electronic properties compared to a Cu(100)c(2×2)-2N/Cu(111). This is because of the different interactions between surface nitrogen and copper atoms from the second layer. The structure of Cu(100)c(2×2)-2N/Cu(100) is presented in Fig. 3.7 [168]. For this structure each surface nitrogen has copper atom from the second layer directly underneath it. However, in the case of a nitride overlayer on a Cu(111) surface, none of copper atoms are positioned directly beneath the surface nitrogen atoms. My analysis, performed after the simple removal of the first layer of copper atoms from the optimised Cu(100)c(2×2)-2N/Cu(111) surface structure, indicates that the surface nitrogen atoms are located mostly in between the copper atoms of the second layer (Fig. 3.6 (inset)). Some of the nitrogen atoms have an adsorption orientation closer to hcp, while others are closer to bridge adsorption side. Only a very small amount of surface nitrogen atoms is close to on top adsorption site. This indicates that the surface nitrogen atoms in pseudo-(100) reconstruction on Cu(100) and Cu(111) have very different electron configurations. The properties of Cu(100)c(2×2)-2N/Cu(100) are clearer and more closely related to that of bulk copper nitride phase (Cu$_3$N) than the Cu(100)c(2×2)-2N/Cu(111) configuration.
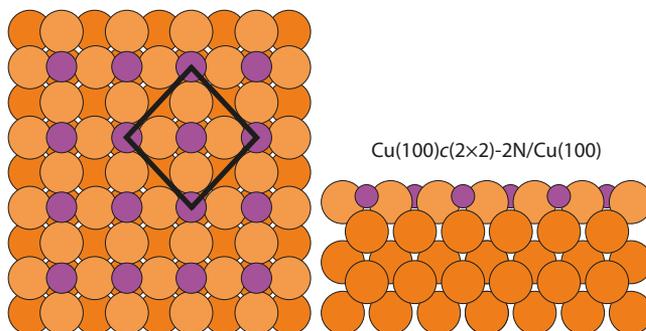

Cu(100)c(2×2)-2N/Cu(100)

Figure 3.7: Ball model for the N-induced structure on Cu(100) surface with a (2×2)-2N overlayer. Orange circles are copper atoms and purple are nitrogen atoms.

Deposition of iron phthalocyanine on Cu(100)c(2×2)-2N/Cu(111)

The structure Cu(100)c(2×2)-2N/Cu(111) has insulating properties (discussed above), so that FePc molecules adsorbed on this layer are expected to be electronically decoupled from the metal surface. In Figure 3.8 the XP spectra of a FePc monolayer on the (a) Cu(100)c(2×2)-2N/Cu(111) and (c) Cu(111) surfaces are presented. Indeed, the FWHM of the C=C peak of FePc on nitrogenated copper is significantly reduced (from 0.75 eV to 0.55 eV). Since the width of the C=C peak is related to both the hybridisation of the FePc molecular states with those of the surface and to an uneven charge distribution in the macrocycle of the molecule, it is clear that the interaction of the molecular overlayer with this support will be modified. It is tempting to assume that

the FePc molecules are fully decoupled from this surface, since we also observe a similar change in the width of the N $1s$ XPS line (Fig. 3.8). In addition, the Fe $2p_{3/2}$ XPS line of FePe on the Cu(100)$c(2\times2)$-2N/Cu(111) broadens significantly. The Fe $2p_{3/2}$ XP spectrum of FePc on the clean Cu(111) is characterised by a low-binding energy narrow peak (707 eV), accompanied by a broad satellite structure at 709.5 eV. This binding energy position and small FWHM have been previously explained as result of charge intake from the surface and quenching of the spin state of the iron ion (S=0) [25]. However, the presence of the nitride layer between FePc and Cu(111) results in a very broad Fe $2p_{3/2}$ spectrum, which is notably broader than that of FePc/Au(111) or FePc/HOPG spectra [18,154]. This result clearly indicates the presence of additional components in the spectrum and that the interaction of the FePc molecular overlayer with the copper nitride on Cu(111) is not as simple as expected.
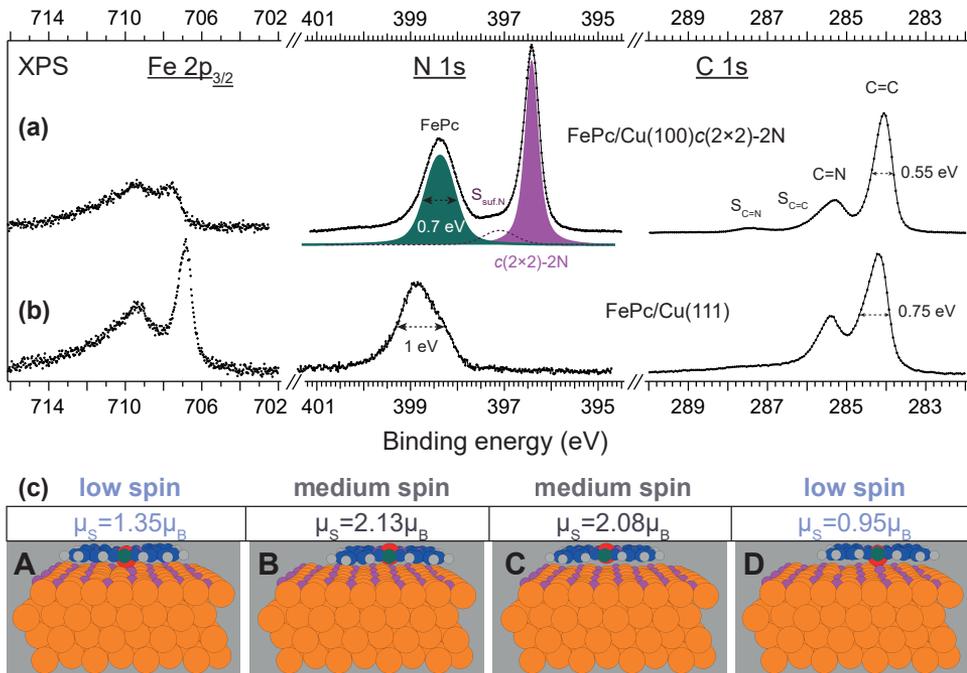
Figure 3.8: Fe $2p_{3/2}$, N $1s$, and C $1s$ XP spectra of a monolayer of FePc deposited on (a) Cu(100)$c(2\times2)$-2N/Cu(111) and (b) Cu(111). (c) Side view of four the most stable adsorption configurations of Cu(100)$c(2\times2)$-2N/Cu(111) identified in the DFT calculations and calculated for each adsorption configuration spin magnetic moment of the iron ion.

DFT calculations on the structure for a single adsorbed FePc molecule, resulted in four of the most stable geometries of FePc on Cu(100)$c(2\times2)$-2N/Cu(111), labelled A to D (Fig. 3.8 (c)). A detailed overview of the adsorption energies of the optimised structures are provided in **Paper III**. Considering the adsorption orientations of these geometries,

in structures A and D, the iron ions are located above the surface nitrogen atoms. In structure B the iron ion is in between copper and nitrogen atoms and in structure C the Fe ion is located directly above the surface copper atom. For configurations B and C, the mean distance to the surface is larger than that for configurations A and D. The stronger interaction between the molecules which have A and D adsorption sites and the support, leads to a shorter mean distance to the surface. Despite the shortened surface-adsorbent distance, the molecules in configurations A and D do not exhibit any structural deformations.

The analysis of the Fe d-orbital pDOS in **Paper III** of structures A and D, show a strong hybridisation of the adsorbate and support states, while this is not the case for structures B and C. This result indicates a strong interaction between the FePc molecule and surface in the case when the Fe ion is located above surface nitrogen atoms. A Bader charge transfer analysis suggests depletion of electron density from the FePc molecules on Cu(100)c(2×2)-2N/Cu(111), which is bigger for adsorption geometries A and D (-0.59 e and -0.71 e) than that for the structures B and C (-0.49 e and -0.52 e, respectively). Furthermore, the calculations of spin magnetic moments indicate that for structures A and D the Fe ion has a low spin state, while for structures B and C, a medium value for the Fe spin state is obtained (Fig. 3.8 (c)).

These results have shown that the adsorption of FePc on nitrogenated Cu(111) leads to co-existence of FePc with both low and medium spin states of Fe ion on a single layer of copper nitride. The different spin states of the Fe center are triggered by the different adsorption sites of the molecule. The FePc molecules which have adsorption site with the Fe ion located above surface nitrogen atoms have reduced spin state due, to a strong surface-adsorbate interaction, while the molecule which adsorb with different surface orientation retain its original medium spin state. The presence on the surface of the FePc molecules with both low and medium spin states of the Fe ion could explain the broad Fe $2p_{3/2}$ XPS line, the width of which is bigger than the previously reported width of FePc in the gas phase [170], or adsorbed on the Au(111) [18] and HOPG [154] surfaces.

This result is quite unexpected, since other studies of similar systems, where the FePc molecule was studied on Cu(100)c(2×2)-2N/Cu(100) [169] the calculations of spin magnetic moment showed that FePc for all adsorption sites only have medium spin state of the iron center. In **Paper III** I argue that this result is triggered by the nature of the support, and, more preciesly, the reconstruction of the copper atoms from the second layer under pseudo-(100) reconstructed layer. As I have described in the previous section, the position of surface nitrogen atoms in Cu(100)c(2×2)-2N overlayer on Cu(111) and Cu(100) is different. When deposited on Cu(100) surface each surface nitrogen atom is located directly above the copper atom. This structure is identical to structure of insulator Cu_3N, where nitrogen has a formal oxidation state of -3. For the Cu(100)c(2×2)-2N/Cu(111) structure nitrogen atoms have different sites on Cu(111) (Fig. 3.8 (inset)), which means that the structure derives from Cu_3N. This effect can slightly increase the oxidation state of nitrogen, which, in turn, might compensate the lacking charge by depleting the electron density from the the FePc molecules.

The surface-induced co-existence of the FePc molecules with different spin states of Fe ion, to my knowledge, is reported for the first time in this work.

Surface–induced modification of ligand-FePc interactions

The previous sections show how the electronic and structural properties of the FePc molecules can be tuned by the nature of the surface the molecules are adsorbed on. In this section I describe how these changes bring differences in further ligand-molecule interactions.

Pyridine adsorption on FePc/Cu(100) $c(2 \times 2)$-2N/Cu(111)

It has been reported previously that pyridine adsorption on Au(111)-supported FePc reduces the spin of the iron ion of the molecule [21]. The quenching of the spin state has been identified from the significantly reduced FWHM of the Fe $2p_{3/2}$ XPS line. The electron donor pyridine creates a bond with the Fe ion and causes a rehybridisation of the open valence states of the Fe center into a closed shell structure (S=0). For the quenched spin state the Zeeman-like splitting is significantly reduced, which results in the narrow Fe $2p$ line.
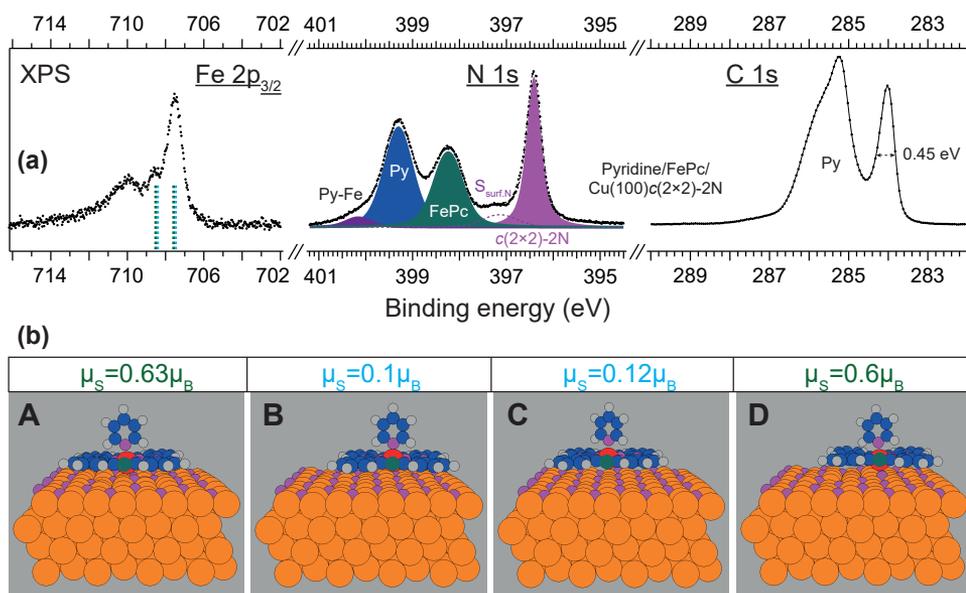
Figure 3.9: (a) Fe $2p_{3/2}$, N 1**s**, and C 1s XP spectra of pyridine (2 L) adsorbed on a monolayer of FePc deposited on a nitrogenated Cu(111) (b) Side view of the four the most stable DFT configurations of FePc/Cu(100) $c(2 \times 2)$-2N/Cu(111) (cf. Fig. 3.8) re-optimised after pyridine adsorption.

In the case of pyridine adsorption on FePc/Cu(100) $c(2 \times 2)$-2N/Cu(111) the Fe $2p_{3/2}$ XP spectrum also shows a significantly narrowed line (Fig. 3.9 (a)) compared to that before pyridine adsorption (Fig. 3.8 (a)). However, the structure of the Fe $2p$ line

still remains complex. In the case of pyridine/FePc/Au(111), only one peak has been observed, while for pyridine/FePc/Cu(100)$c(2\times2)$-2N/Cu(111) two peaks of different intensity at 707.4 and 708.3 eV, accompanied by a characteristic for FePc satellite structure at 709.9 eV, is observed. This behaviour can be understood from the presence of the different types of adsorbates, as discussed in the section above. These different types remain even after pyridine adsorption, but they have different spin magnetic moments and electron structures (Fig. 3.9 (b)). The presence in XP spectra of two distinguishable Fe $2p_{3/2}$ peaks supports the idea of the existence of different spin states related to the adsorption in different surface sites.

Oxygen–FePc interaction as a result of the surface trans effect

In **Paper IV** the interaction of molecular oxygen with FePc supported on Au(111) and Cu(111) at close to realistic oxygen pressures (0.2 - 0.33 mbar) have been studied. As it has been underlined previously and is shown in these studies, the surface has a tremendous impact on the reactivity of the FePc molecule. XPS data analysis in **Paper IV** show that there is no significant interaction of molecular oxygen with Au(111)-supported FePc. In contrast, when FePc is deposited on the more reactive Cu(111) surface, I have observed significant changes in the photoemission spectra of all core levels upon molecular oxygen exposure (Fig. 3.10 (c-d)). The changes in the C $1s$ core level spectra indicate a strong interaction between oxygen and the pyrrole rings of FePc. The shape of the Fe $2p$ (**Paper IV**) line suggests an electronic decoupling of the iron ion from the surface and an oxidation of the central iron ion as it shifts significantly to a higher binding energy, and thus indicative of a depletion of electron density on it. These results indicate that the variant reactivity of FePc compounds on these two surfaces with respect to molecular oxygen is a result of the different electronic coupling of the FePc molecules to the surfaces.
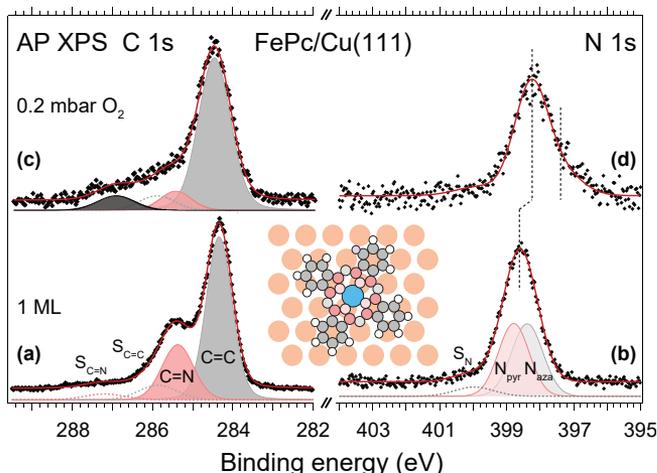

Figure 3.10: XP spectra (C $1s$ and N $1s$) of a monolayer of FePc adsorbed on Cu(111) (a-b) before and (c-d) after exposure to molecular oxygen (0.2 mbar).

The reactivity and stability of supported NHC-Pd complexes

In **Paper V** I investigate surface-induced modifications of another type of late transition metal complex, - N-heterocyclic carbene palladium complex. The structures of two new NHC-Pd complexes studied in this work are presented in Fig. 1.2. As it has been discussed in the introduction chapter of this thesis, NHC-Pd complexes are well-known homogeneous catalysts that has shown high selectivity and activity under mild reaction conditions. But it is also well-known that the recycling and separation problem from the reaction media are major drawbacks of homogeneous catalysis. Therefore, in **Paper V** I have studied heterogenised via anchoring to silicon wafers NHC-Pd complexes **1** and **2** by a combination of XA and XP spectroscopic studies, with theoretical (DFT) support. The N K-edge XA spectra were recorded in detail at N $1s$ absorption edge at different angles between incidence angle of x-rays and surface normal, to identify adsorption geometries of the complexes **1** and **2** on the surface (Fig. 3.11).

The analysis of the contributions of different π^* resonances in XA spectra, supported by DFT calculations of excitation probabilities to the lowest unoccupied molecular orbital (LUMO) of imidazole and chloropyridine in complexes, indicates that heterogenisation of complexes leads to breaking ClPy-Pd bond in of the complexes. This can be seen from the low intensity contribution of π^* resonance, which corresponds to chloropyridine. The expected ClPy:Im ratio from stoichiometry of both complexes is 1:2, but after taking into account that the chloropyridine to imidazole oscillator strengths are quite different, due to different value of transition matrix element, the calculations suggest that 1:1 ratio is expected. By integrated intensities of π^* resonance of chloropyridine and imidazole I have estimated the amount of intact complex **1** after its immobilisation on the surface to be 15%. Analysis of XAS data of complex **2** suggests that there is less than 1% of intact complexes **2** on the surface.

One of the main scopes of the X-ray absorption investigation presented in **Paper V** is the determination of the orientation of the supported complex **1** and **2** to identify the nature of adsorption of the complexes on the surface. The orientation of the compounds can be calculated from the intensity variations of both π^* and σ^* resonances with variation of light incidence angle. However, I have considered only π^* resonances due to their narrow line shapes and consequently, more accurate analysis. The analysis of intensity variation of the first π^* resonance of imidazole with the incidence angle of x-rays shows that intact and non-intact complex **1** have mutually excluding adsorption orientations. This means that when an intact complex **1** has an imidazole ring oriented perpendicular to the surface, the orientation imidazole ring of the non-intact complex **1** orients towards being parallel to the surface, and vice versa. The analysis of XP spectra of complex **1** suggests orientation of non-intact complexes with imidazole ring perpendicularly to the surface. This is due to possible creation of the bond between palladium ion and surface oxygen. This orientation of non-intact complex **1** suggests that the intact complex **1** is laying or standing with a small small angle to the surface.

These experiments have been performed to apply this knowledge for immobilisation of the corresponding complexes **1** and **2** on a mesoporous silica (SBA-15). To check the catalytic activity of heterogenised complex **1** immobilised on SBA-15 material,
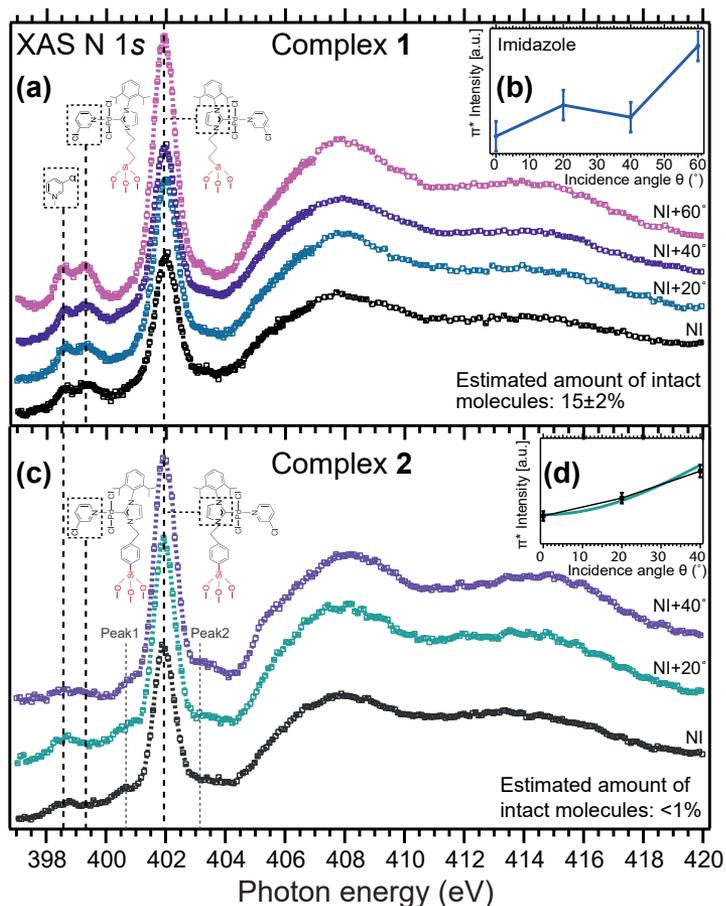
Figure 3.11: N 1*s* X-ray absorption spectra for (a) complexes **1** and (c) complex **2** recorded at different angles between surface normal and incidence angle of x-rays; (b and g) integrated XA intensities of π^* resonance of imidazole peak as a function of incidence angle.

the model reaction of 2-phenylpyridine acetoxylation was performed. The results of gas chromatography analysis showed that only 10% of the substrate was converted to acetoxylated product. This can be due to the partial decomposition of the catalyst on the surface of the SBA-15 material, as in the case of complex **1** anchored to silicon wafer studied in **Paper V**, and its further deactivation. This result is in perfect agreement with the results of the complexes supported on silicon wafer, thus, the obtained knowledge can be used for improving the properties of the catalyst support, to increase the yield of the product upon catalytic reaction.

CHAPTER 4

Concluding remarks and outlook

The work presented in this thesis demonstrates that the molecular properties of organic-metal complexes on surfaces clearly depend on the nature of the support they are adsorbed on. This knowledge is essential for future generation of molecule-based electronic devices, because the unique properties of the building blocks of these potential application depend critically on the properties of the surface the molecules are adsorbed on.

In **Paper I** I have shown that on clean Cu(111) the reactivity of the surface, even at room temperature, triggers electronic and structural changes in the FePc molecule such, as electron charge transfer and symmetry breaking. The temperature elevation of Cu(111)-supported FePc to a compound-specific temperature (300-320°C) induces surface chemical reactions, such as a homocoupling reaction, in which the outer and middle carbon atoms in benzo moieties loose one or two hydrogen atoms and become further involved in the reaction of neighboring molecules (**Paper II**). Previously these modifications, both at room and elevated temperatures, have been observed only by imaging techniques, while I have shown that these effects are corroborated in XP and XA spectroscopy data.

Continuing my extensive studies of surface-induced modifications of transition metal compounds, in **Paper III**, I have also investigated the influence of a single layer of copper nitride on the properties of the FePc molecules. Contrary to expectations, combined theory and XPS investigation show that the deposition of the FePc molecules on a single layer of copper nitride on Cu(111) does not lead to a full electronic decoupling of the molecules from the surface. The adsorption of FePc on pseudo-Cu(100)$c(2\times2)$-2N/Cu(111) leads to the occurrence of the FePc molecules with medium and low spin states of iron ion, depending on the adsorption site.

In **Papers III** and **IV** I show how support can alter ligand-FePc interaction. The pyridine adsorption on Cu(100)$c(2\times2)$-2N/Cu(111)-supported FePc results in an expected reduction in the Fe ion spin. Interestingly, different types of adsorbates with different spin caused by FePc deposition on Cu(100)$c(2\times2)$-2N/Cu(111), persist even after pyridine adsorption but have either reduced or quenched Fe spin. In **Paper IV** I show that the different reactivity of FePc with respect to molecular oxygen is a surface-induced effect.

In **Paper V**, the structure, stability and surface orientation of two NHC-Pd complexes supported on a silicon wafer have been characterised by combining XAS and XPS and these experiments were further supported by DFT calculations. Our results indicate only

15% of the complexes immobilised on the surface though a flexible linker, stay intact on the surface. The complexes immobilised on more rigid linker almost fully dissociate. The next logical step of the research on these complexes will be improving the surface used for heterogenizing the NHC-Pd complexes, since the nature of the surface-induced decomposition is now fairly well understood.

As expected from a thesis, several open questions arise from the analysis of the work presented that would make for intriguing follow up projects. In **Paper I** I have shown that the symmetry reduction effect has its spectroscopic fingerprint in the recorded XPS data, however, the measurement have been performed only for one type of metal phthalocyanine molecule - FePc. In the pioneering work by Chang et al. [34], where the symmetry breaking was demonstrated for the first time, it was reported that the symmetry reduction is much more pronounced for CuPc and CoPc molecule, while it is only faintly present for FePc. Therefore, an investigation of widths of XPS lines for these different metal phthalocyanine molecules, as a function of calculated charge transfer from the surface, could provide a detailed insight into the symmetry reduction impact on XP spectra broadening. These effects appear to depend on the properties of the metal centre of the compound.

In addition, since in **Paper IV** I show that the catalytic activity of the FePc molecule can be surface-tuned, the organometallic sheet of FePc can potentially be used for CO oxidation reaction. Fig. 4.1 shows the recorded data of a monolayer of FePc on Cu(111) during the reaction with a mixture O_2+CO at pressure of 0.2 mbar. At 100°C, the occurrence of the peak at 535.4 eV binding energy, in the O $1s$ XP spectrum , is indicative of the gas phase CO_2 production. This result *seems* to show that FePc is a surface-tuned catalyst for CO_2 production. However, very recent publications of AP XPS studies of CO oxidation reaction on Cu(111) [171, 172] suggest that the CO_2 peak may not be due to FePc, but is rather due to CO oxidation on reconstructed Cu(111) by pre-adsorbed oxygen. Therefore, the CO oxidation reaction on metal phthalocyanines by AP XP spectroscopy should be studied in more detail for MPcs supported on the surfaces, which have a strong hybridisation with the molecules, but no reactivity towards CO oxidation.
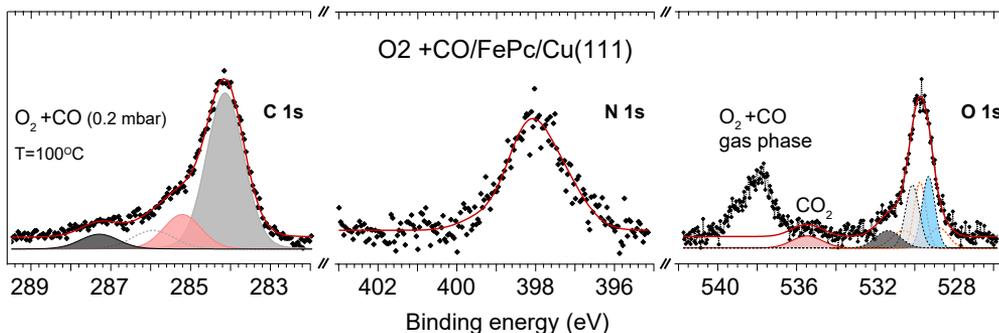

Figure 4.1: APXP spectra (C $1s$ and N $1s$) of a monolayer of FePc on Cu(111) during the reaction with mixture O_2(30%)+CO(70%) (0.2 mbar) at (a) 100°C and (b) 200°C, respectively.

Acknowledgements

Firstly, I would like to show my gratitude and appreciation to my supervisor, Prof Achim Schnadt for allowing me to be myself, take control over my research, and make it my own with the occasional directional prod in the right way. I always felt independent, but never abandoned, which I am very grateful for. Thank you so much for showing me that it is not that scary to jump in at the deep end and learn by a hands-on approach during my numerous experiments. I gained a vast amount of my experience and knowledge thanks to your guidance and help.

Secondly, I would like to thank my co-supervisor Dr Jan Knudsen for helping me with my experiments and staying all those long night-shifts at MAX-lab and measuring countless spectra, which build the basis of this thesis. I also thank my second co-supervisor, Prof Ola Wendt for all our SMALL group meeting discussions, in which your participation and opinion as organic chemistry expert is highly appreciated.

Prof Stacey Ristinmaa Sörensen for our yearly progress discussions, each time they have made me to look on my research from a slightly different perspective, Dr Mathieu Gisselbrecht for inspiring me to do even better presentations, Dr Danny Mannix for proof-reading this thesis and scientific advices, Prof Edvin Lundgren for organizing amazing Kick-off meetings in all those outstanding locations, Dr Johan Gustafson for all software help and advice I have got, Dr Karina Schulte for your interest and participation in my experiments and all the advice I have got during our common beamtimes.

I would like to thank to all my inspiring and talented colleagues - Shilpi Chaudhary, for your support during our countless experiments together, your kindness, and friendship; Ekaterina Bolbat, thank you for our friendship during all these years and all our really great conference trips together; Niclas Johansson, for our scientific/non-scientific discussions and all kindly provided by you Igor macros; Lisa Rullik for being such an amazing cook; Natalia Martin, Elin Grånäs, Erik Månson, Jovanna Colvin, Olof Persson, and Erik Malm, for being great office mates; Erik Mårsell, for moral support during my thesis writing; Andrea Troian, for our coffee breaks which made tough days easier; Martin Hjort, for ghost haunting; Payam Shayesteh, Tripta Kamra, Ashley R. Head, Sarah McKibbin, Misha Shipilin, Jonas Evertsson, Sara Blomberg, Johan Knutsson, Noelle Walsh, Sofie Yngman, Chu Chu Zhang, Estephania Lira, Lindsay Merte, Alif Arman, Bart Oostenrijk, Rainer Timm, Andreas Schaefer, Anders Mikkelsen, and Jesper Wallentin, for being great colleagues and interesting people, all of you contribute to warm Sljus atmosphere; Shabnam Oghbaiee is acknowledged for proving empirically for me that the gorilla glass is not unbreakable; and Anna Sankari, for our interesting discussions.

Thank you to all my amazing collaborators and co-authors: Johann Lüder, Prof Barbara Brena, Jan Rusz, Alissa Wiengarten, Prof Willi Auwärter, Felix Bischoff, Yuanqin He, Dr Knud Seufert, Prof Johannes Barth, Shiri Burema, Prof Marie-Laure Bocquet, Ieva Bidermane, Prof Carla Puglia, Prof Roberto Otero, Prof James O'Shea,

Bibliography

[1] R. Feynman, *There's Plenty of Room at the Bottom*, Caltech Engineering and Science, Vol. 23:5 (1960) 22 - 36.

[2] R. P. Linstead, *Phthalocyanines. Part I. A New Type of Synthetic Colouring Matters*, J. Chem. Soc. 1016 (1934).

[3] A. Braun and J. Tcherniac, *The Products of the Action of Acet-Anhydride on Phthalamide*, Berichte der Deutschen Chemischen Gesellschaft 40 (1907) 2709 - 2714.

[4] G. T. Byrne, R. P. Linstead, and A. R. Lowe, *Phthalocyanines. Part II. The Preparation of Phthalocyanine and Some Metallic Derivatives from O-Cyanobenzene and Phthlimide*, J. Chem. Soc. 1017 (1934).

[5] R. P. Linstead and A. R. Lowe, *Phthalocyanines. Part III. Preliminary Experiments on the Preparation of Phthalocyanines from Phthalonitride*, J. Chem. Soc. 1022 (1934).

[6] C. E. Dent and R. P. Linstead, *Phthalocyanines. Part IV. Copper phthalocyanines*, J. Chem. Soc. 1027 (1934).

[7] R. P. Linstead and A. R. Lowe, *Phthalocyanines. Part V. The Molecular Weight of Magnesium Phthalocyanine*, J. Chem. Soc. 1031 (1934).

[8] C. E. Dent, R. P. Linstead, and A. R. Lowe, *Phthalocyanines. Part VI. The Structure of the Phthalocyanines*, J. Chem. Soc. 1033 (1934).

[9] J. M. Robertson, *An X-Ray Study of the Structure of the Phthalocyanines. Part I. The Metal-free, Nickel, Copper, and Platinum Compounds*, J. Chem. Soc. (1934) 615.

[10] Lionel R. Milgrom, *The Colours of Life - An Introduction to the Chemistry of Porphyrins and Related Compounds*, Oxford University Press, New York, 1997.

[11] N. B. McKeown, *Phthalocyanine Materials: Synthesis, Structure and Function*, Cambridge University Press, Cambridge, 1998.

[12] F. H. J. Figge, G. S. Weiland, and L. O. J. Manganiello, *Cancer Detection and Therapy. Affinity of Neoplastic, Embryonic, and Traumatized Tissues for Porphyrins and Metalloporphyrins*, Proc. of the Soc. for Exp. Biol. and Med.68 (1948) 640 - 641.

[13] E. Benhur and I. Rosenthal, *The Phthalocyanines: a New Class of Mammalian Cells Photosensitizers with a Potential for Cancer Phototherapy*, Int. J. of Radiat. 47 (1985) 145 - 147.

[14] E. Benhur and I. Rosenthal, *Phthalocyanines - Properties and Applications*, Vol. 1, eds. C.C. Lenznoff and A. B. P. Lever, VCH Publishers, Inc., New York, 1989.

[15] C. N. Lunardi and A. C. Tedesco, *Synergic Photosensitizers: A New Trend in Photodynamic Therapy*, Curr. Org. Chem. 9 (2005) 813 - 821.

[16] J. P. Taquet, C. Frochot, V. Manneville, and M. Barberi-Heyob, *Phthalocyanines Covalently Bound to Biomolecules for a Targeted Photodynamic Therapy*, Curr. Org. Chem. 14 (2007) 1673 - 1687.

[17] N. Nombona, K. Maduray, E. Antunes, A. Karsten, and T. Nyokong, *Synthesis of Phthalocyanine Conjugates with Gold Nanoparticles and Liposomes for Photodynamic Therapy*, J. Photochem. Photobiol. B: Biol. 107 (2012) 35-44.

[18] C. Isvoranu, B. Wang, K. Schulte, E. Ataman, J. Knudsen, J. N. Andersen, M. L. Bocquet, and J. Schnadt, *Tuning the Spin State of Iron Phthalocyanine by Ligand Adsorption*, J. Phys.: Condens. Matter 22 (2010) 472002.

[19] C. Isvoranu, B. Wang, E. Ataman, K. Schulte, J. Knudsen, J. N. Andersen, M. L. Bocquet, and J. Schnadt, *Ammonia Adsorption on Iron Phthalocyanine on Au(111): Influence on AdsorbateSubstrate Coupling and Molecular Spin*, J. Chem. Phys. 134 (2011) 114710.

[20] C. Isvoranu, J. Knudsen, E. Ataman, K. Schulte, B. Wang, M. L. Bocquet, J. N. Andersen, and J. Schnadt, *Adsorption of ammonia on multilayer iron phthalocyanine*, J. Chem. Phys. 134 (2011) 114711.

[21] C. Isvoranu, B. Wang, E. Ataman, K. Schulte, J. Knudsen, J. N. Andersen, M. L. Bocquet, and J. Schnadt, *Pyridine Adsorption on Single-Layer Iron Phthalocyanine on Au(111)*, J. Phys. Chem. C 115 (2011) 20201 - 202008.

[22] C. Isvoranu, B. Wang, E. Ataman, J. Knudsen, K. Schulte, J. N. Andersen, M. L. Bocquet, and J. Schnadt, *Comparison of the Carbonyl and Nitrosyl Complexes Formed by Adsorption of CO and NO on Monolayers of Iron Phthalocyanine on Au(111)*, J. Phys. Chem. C 115 (2011) 24718 - 24727.

[23] C. Wäckerlin, D. Chylarecka, A. Kleibert, K. Müller, C. Iacovita, F. Nolting, T. A. Jung, and N. Ballav, *Controlling Spins in Adsorbed Molecules by a Chemical Switch*, Nature Commun. 1 (2010) Art. No. 61.

[24] N. Tsukahara, E. Minamitani, Y. Kim, M. Kawai, and N. Takagi, *Controlling Orbital-Selective Kondo Effects in a Single Molecule through Coordination Chemistry*, J. Chem. Phys. 141 (2014) 054702.

[25] N. Tsukahara, K. Noto, M. Ohara, S. Shiraki, and N. Takagi, *Adsorption-Induced Switching of Magnetic Anisotropy in a Single Iron(II) Phthalocyanine Molecule on an Oxidized Cu(110) Surface*, Phys. Rev. Let. 102 (2009) 167203.

[26] F. Petraki, H. Peisert, I. Biswas, and T. Chasśe, *Electronic Structure of Co-Phthalocyanine on Gold Investigated by Photoexcited Electron Spectroscopies: Indication of Co Ion-Metal Interaction*, J. Phys. Chem. C 114 (2010) 17638 - 17643.

[27] F. Petraki, H. Peisert, F. Latteyer, U. Aygül, A. Vollmer, and T. Chasśe, *Impact of the 3d Electronic States of Cobalt and Manganese Phthalocyanines on the Electronic Structure at the Interface to Ag(111)*, J. Phys. Chem. C 115 (2011) 21334 21340.

[28] M. Schmidt, A. Kaftan, H.-P. Steinrück, and J. M. Gottfried, *The electronic structure of cobalt(II) phthalocyanine adsorbed on Ag(111)*, Surf. Sci. 606 (2012) 945 - 949.

[29] E. Salomon, P. Amsalem, N. Marom, M. Vondracek, L. Kronik, N. Koch, and T. Angot, *Electronic structure of CoPc adsorbed on Ag(100): Evidence for molecule-substrate interaction mediated by Co 3d orbitals*, Phys. Rev. B 87 (2013) 075407.

[30] F. Petraki, H. Peisert, Y. Aygül, F. Latteyer, J. Uihlein, A. Vollmer, and T. Chasśe, *Electronic Structure of FePc and Interface Properties on Ag(111) and Au(100)*, J. Phys. Chem. C 116 (2012) 11110 11116.

[31] Y. Wang, X. Ge, C. Manzano, J. Kröger, R. Berndt, W. A. Hofer, H. Tang, and J. Cerda, *Supramolecular Patterns Controlled by Electron Interference and Direct Intermolecular Interactions*, J. Am. Chem. Soc. 131 (2009) 10400 - 10402.

[32] B. W. Heinrich, C. Iacovita, T. Brumme, D.-J. Choi, L. Limot, M. V. Rastei, W. A. Hofer, J. Kortus, and J.-P. Bucher, *Direct Observation of the Tunneling Channels of a Chemisorbed Molecule*, J. Phys. Chem. Lett. 1 (2010) 1517 - 1523.

[33] J. D. Baran and J. A. Larsson, *Theoretical Insights into Adsorption of Cobalt Phthalocyanine on Ag(111): A Combination of Chemical and van der Waals Bonding*, J. Phys. Chem. C 117 (2013) 23887 - 23898.

[34] S.-H. Chang, S. Kuck, J. Brede, L. Lichtenstein, G. Hoffmann, and R. Wiesendanger, *Symmetry Reduction of Metal Phthalocyanines on Metals*, Phys. Rev. B 78 (2008) 233409.

[35] H. Karacuban, M. Lange, J. Schaffert, O. Weingart, Th. Wagnera, and R. Möller, *Substrate-Induced Symmetry Reduction of CuPc on Cu(111): An LT-STM Study*, Surf. Sci. 603 (2009) L39 - L43.

[36] A. Mugarza, N. Lorente, P. Ordejón, C. Krull, S. Stepanow, M.-L. Bocquet, J. Fraxedas, G. Ceballos, and P. Gambardella, *Orbital Specific Chirality and Homochiral Self-Assembly of Achiral Molecules Induced by Charge Transfer and Spontaneous Symmetry Breaking*, Phys. Rev. Lett. 105 (2010) 115702.

[37] R. Cuadrado, J. I. Cerdá, Y. Wang, G. Xin, R. Berndt, and H. Tang, *CoPc Adsorption on Cu(111): Origin of the C4 to C2 Symmetry Reduction*, J. Chem. Phys. 133 (2010) 154701.

[38] T. Niu, J. Zhang, and W. Chen, *Molecular Ordering and Dipole Alignment of Vanadyl Phthalocyanine Monolayer on Metals: The Effects of Interfacial Interactions*, J. Phys. Chem. C 118 (2014) 4151 - 4159.

[39] M. Toader, P. Shukrynau, M. Knupfer, D. R. T. Zahn, and M. Hietschold, *Site-Dependent Donation/Backdonation Charge Transfer at the CoPc/Ag(111) Interface*, Langmuir 28 (2012) 13325 - 13330.

[40] S. Fortuna, P. Gargiani, M. G. Betti, C. Mariani, A. Calzolari, S. Modesti, and S. Fabris, *Molecule-Driven Substrate Reconstruction in the Two-Dimensional Self-Organization of Fe-Phthalocyanines on Au(110)*, J. Phys. Chem. C 116 (2012) 6251 - 6258.

[41] W.-H. Soe, C. Manzano, H. S. Wong, and C. Joachim, *Mapping the First Electronic Resonances of a Cu Phthalocyanine STM Tunnel Junction*, J. Phys.: Condens. Matter 24 (2012) 354011.

[42] T. Lukasczyk, K. Flechtner, L. R. Merte, N. Jux, F. Maier, J. M. Gottfried, and H.-P. Steinrück, *Interaction of Cobalt(II) Tetraarylporphyrins with a Ag(111) Surface Studied with Photoelectron Spectroscopy*, J. Phys. Chem. C 111 (2007) 3090.

[43] M. Häming, C. Scheuermann, A. Schöll, F. Reinert, and E. Umbach, *Coverage Dependent OrganicMetal Interaction Studied by High-Resolution Core Level Spectroscopy: SnPc (sub)monolayers on Ag(111)*, J. Elec. Spec. Rel. Phen. 174 (2009) 59.

[44] Y. Bai, F. Buchner, I. Kellner, M. Schmid, F. Vollnhals, H.-P. Steinrück, H. Marbach, and J. M. Gottfried, *Adsorption of Cobalt (II) Octaethylporphyrin and 2H-Octaethylporphyrin on Ag(111): New Insight into the Surface Coordinative Bond*, New J. Phys. 11 (2009) 125004.

[45] I. Kröger, B. Stadtmüller, C. Stadler, J. Ziroff, M. Kochler, A. Stahl, F. Pollinger, T.-L. Lee, J. Zegenhagen, F. Reinert, and C. Kumpf, *Submonolayer Growth of Copper-Phthalocyanine on Ag(111)*, New J. Phys. 12 (2010) 083038.

[46] P. Gargiani, M. Angelucci, C. Mariani, and M. G. Betti, *Metal-Phthalocyanine Chains on the Au(110) Surface: Interaction States versus d-metal States Occupancy*, Phys. Rev. B 81 (2010) 085412.

[47] M. G. Betti, P. Gargiani, R. Frisenda, R. Biagi, A. Cossaro, A. Verdini, L. Floreano, and C. Mariani, *Localized and Dispersive Electronic States at Ordered FePc and CoPc Chains on Au(110)*, J. Phys. Chem. C 114 (2010) 21638.

[48] B. Stadtmüller, I. Kröger, F. Reinert, and C. Kumpf, *Submonolayer Growth of CuPc on Noblemetal Surfaces*, Phys. Rev. B 83 (2011) 085416.

[49] M. Schmid, J. Zirzlmeier, H.-P. Steinrück, and J. M. Gottfried, *Interfacial Interactions of Iron(II) Tetrapyrrole Complexes on Au(111)*, J. Phys. Chem. C 115 (2011) 17028.

[50] M. Toader, M. Knupfer, D. R. T. Zahn, and M. Hietschold, *Initial Growth at the F16CoPc/Ag(111) Interface*, Surf. Sci. 605 (2011) 1510.

[51] F. Bischoff, K. Seufert, W. Auwärter, S. Joshi, S. Vijayaraghavan, D. Écija, K. Diller, A. C. Papageorgiou, S. Fischer, F. Allegretti, D. A. Duncan, F. Klappenberger, F. Blobner, R. Han, and J. V. Barth, *How Surface Bonding and Repulsive Interactions Cause Phase Transformations: Ordering of a Prototype Macrocyclic Compound on Ag(111)*, ACS Nano 7, 3139 (2013).

[52] I. Swart, T. Sonnleitner, and J. Repp, *Charge State Control of Molecules Reveals Modification of the Tunneling Barrier with Intramolecular Contrast*, Nano Lett. 11 (2011) 1580.

[53] C. Uhlmann, I. Swart, and J. Repp, *Controlling the Orbital Sequence in Individual Cu-Phthalocyanine Molecules*, Nano Lett. 13 (2013) 777.

[54] Y. Y. Zhang, S. X. Du, and H.-J. Gao, *Binding Configuration, Electronic Structure, and Magnetic Properties of Metal Phthalocyanines on a Au(111) Surface Studied with ab initio Calculations*, Phys. Rev. B 84 (2011) 125446.

[55] A. Mugarza, R. Robles, C. Krull, R. Korytár, N. Lorente, and P. Gambardella, *Electronic and Magnetic Properties of MoleculeMetal Interfaces: Transition-Metal Phthalocyanines Adsorbed on Ag(100)*, Phys. Rev. B 85 (2012) 155437.

[56] Y. Okawa, S. K. Mandal, C. Hu, Y. Tateyama, S. Goedecker, S. Tsukamoto, T. Hasegawa, J. K. Gimzewski, and M. Aono, *Chemical Wiring and Soldering Toward All-Molecule Electronic Circuitry*, J. Am. Chem. Soc. 133 (2011) 8227 - 8233.

[57] P. Liljeroth, J. Repp, and G. Meyer, *Current-Induced Hydrogen Tautomerization and Conductance Switching of Naphthalocyanine Molecules*, Science 317 (2007) 1203 - 1206.

[58] R. Vincent, S. Klyatskaya, M. Ruben, W. Wernsdorfer, and F. Balestro, *Electronic read-out of a single nuclear spin using a molecular spin transistor*, Nature 488 (2012) 357 - 360.

[59] J. D. Baran and J. A. Larsson, *Inversion of the Shuttlecock Shaped Metal Phthalocyanines MPc (M = Ge, Sn, Pb)- A Density Functional Study*, Phys. Chem. Chem. Phys. 12 (2010) 6179 - 6186.

[60] N. J. Tao, *Molecular Switches: Pushing the Right Button*, Nat. Chem. 1 (2009) 108 - 109.

[61] T. Komeda, H. Isshiki, J. Liu, Y.-F. Zhang, N. Lorente, K. Katoh, B. K. Breedlove, and M. Yamashita, *Observation and Electric Current Control of a local spin in a Single-Molecule Magnet*, Nat. Commun. 2 (2011) 217 - 223.

[62] J. Manassen and A. Bar-Ilan, *Metal Complexes of Phthalocyanine and $\alpha, \beta, \gamma, \sigma$-Tetraphenyl Porphyrin as Heterogeneous Catalysts in Oxidative Dehydrogenation. Correlation between Catalytic Activity and Redox Potential*, J. Cat. 17 (1970) 86 - 92.

[63] J. R. Darwent, *Photoreduction of Methyl Viologen in Micellar Solutions Sensitized by Zinc Phthalocyanine*, J. Chem. Soc. Chem. Comm. (1980) 805 - 807.

[64] A. Harriman and M-C. Richoux, *Attempted Photoreduction of Hydrogen using Sulphoph-thalocyanines as Chromophores for Three-component Systems*, J. Chem. Soc.-Faraday II 76 (1980) 1618.

[65] M. Toledo, Alzira M. S. Lucho, and Y. Gushikem, *In situ Preparation of Co Phthalocyanine on a Porous Silica Gel Surface and the Study of the Electrochemical Oxidation of Oxalic Acid*, J. Mat. Sci. 39 (2004) 6851 - 6854.

[66] J. C. Obirai and T. Nyokong, *Thiol Oxidation at 2-Mercaptopyrimidine-appended Cobalt Phthalocyanine Modified Glassy Carbon Electrodes*, J. Electroanal. Chem. 600 (2007) 251 - 256.

[67] T. W. Lyons and M. S. Sanford, *Palladium-Catalyzed Ligand-Directed C-H Functionaliza-tion Reactions*, Chem. Rev. 110 (2010) 1147 - 1169.

[68] C. W. Jones, *On the Stability and Recyclability of Supported Metal-Ligand Complex Catalysts: Myths, Misconceptions and Critican Research Needs*, Top. Catal 53 (2010) 942 -952.

[69] M. P. Seah and W. A. Dench, *Quantitative Electron Spectroscopy of Surfaces: A Standard Data Base for Electron Inelastic Mean Free Path in Solids*, Surf. Inter. Anal., 12 (1979).

[70] J. Schnadt, J. N. O'Shea, L. Patthey, J. Krempaský, N. Mårtensson, and P. A. Brühwiler, *Alignment of valence photoemission, x-ray absorption, and substrate density of states for an adsorbate on a semiconductor surface*, Physical Review B 67 (2003) 235420.

[71] K. Siegbahn, *Electron Spectroscopy for Molecules and Condensed Matter - An Overview*, J. Elec. Spec. Rel. Phen., 36 (1985) 113-129.

[72] http://www.nobelprize.org/nobel_prizes/physics/laureates/1981/, accessed Sep. 25, 2014.

[73] K. Siegbahn, C. Nordling, R. Fahlman, R. Nordberg, K. Hamrin, J. Hedman, G. Johansson, T. Bergmark, S.-E. Karlsson, I. Lindgren, and B. Lindberg, *ESCA: Atomic, Molecular and Solid Structure Studies by Means of Electron Spectroscopy*, Nova Acta Regiae Soc. Sci., Upsaliensis, Ser. IV (1967) Vol. 20.

[74] K. Oura, V. G. Lifshits, A. A. Saranin, A. V. Zotov, and M. Katayama, *Surface Science: An Introduction (Advanced Texts in Physics)*, New York: Springer, 2010.

[75] David J. Griffiths, *Introduction to Quantum Mechanics*, Second Edition, Pearson Education International, Printed in the United States of America, 2005.

[76] C. S. Fadley, *Electron Spectrocopy: Theory, Techniques and Applications*, Vol. 2, ed. by C. R. Brundle, A. D. Baker, Academic, New York, 1978.

[77] Leonard I. Schiff, *Quantum Mechanics*, Third Edition, McGraw-Hill, Inc., Printed in the United States of America, 1995.

[78] B. H. Bransden and C. J. Joachain, *Quantum Mechanics*, Second Edition, Pearson Education Limited, Harlow England, 2000.

[79] S. Hüfner, *Photoelectron Spectroscopy: Principles and Applications*, Third Edition, Springer - Verlag Berlin Heidelberg New York, 2003.

[80] N. Mårtensson, *Core Level Spectroscopies Applied to Surfaces and Adsorbates*, Ecole Polytechnique Federale de Lausanne, Lausanne, 1994.

[81] J. N. Andersen, D. Hennig, E. Lundgren, M. Methfessel, R. Nyholm, M. Scheffier, *Surface core-level shifts of some 4d-metal single-crystal surfaces: Experiments and ab initio calculations*, Physical Review B 50 (1994) pp. 17525-17533.

[82] A. E. Lindh and O. Lundquist, *Shake-up and Shake-off Structures in Core Level Photoemission Spectra from Adsorbates*, Ark. Mat. Astron. Fys. 18 No 3, 14 (1924) 35.

[83] A. Faessler, *X-ray emission and the chemical bond*, In Proceedings of the Tenth Colloquium Spetroscopicum Internationale, ed. E. R. Lippincott and M. Margoshes, Sparton Books, Washington, D. C. (1963) pp. 307-319.

[84] Y. Cauchois, *Spectres et laison chimique*, J. Chim. Phys. 51 (1954) D76-88.

[85] W. Eberhardt (Ed.) with contributions by A. M. Bradshaw, W. Eberhardt, H.-J. Freund, F. M. Hoffmann, H. Kuhlenbeck, N. Mårtensson, D. Menzel, A. Nilsson, G. P. Williams, D. P. Woodruff, and W. Wurth, *Applications of Synchrotron Radiation: High-Resolution Studies of Molecules and Molecular Adsorbates on Surfaces*, Chapter 3, Springer-Verlag Berlin Heidelberg New York, 1995.

[86] N. Mårtensson and A. Nilson, *Core-Level Line Shapes of Adsorbates: Effects of Electronic and Vibrational Excitations*, J. Elec. Spec. Rel. Phen. 52 (1990) 1-46.

[87] J. Michael Hollas, *Modern Spectroscopy*, Fourth Edition, John Wiley & Sons, Ltd, The Atrium, Southern Gate, Chichester, West Sussex PO19 8SQ, England, 2004.

[88] A. N. Hattori, K. Hattori, and H. Daimon, *X-ray photoelectron spectroscopy of SPE-grown bcc-Fe, polycrystal and $\beta - FeSi_2$ phases on Si(111) surfaces*, Surf. Int. Anal. 40 (2008) 988-992.

[89] A. Stenborg, J. N. Andersen, O. Björneholm, A. Nilsson, and N. Mårtensson, *Core Level Line Width of Metallic Systems*, J. Elec. Spec. Rel. Phen. 52 (1990) 47-48.

[90] S. Mähl, M. Neumann, S. Dieckhoff, V. Schlett, and A. Baalmann, *Characterisation of the VG ESCALAB instrumental broadening functions by XPS measurements at the Fermi edge of silver*, J. Elec. Spec. Rel. Phen. 85 (1997) 197-203.

[91] J. Stöhr, R. Jaeger, and J. J. Rehr, *Transition from Adiabatic to Sudden Core-Electron Excitation: N_2 on Ni*(110), Phys. Rev. Lett. 51 (1983) 821.

[92] B. K. Agarwal, *X-ray Spectroscopy: An Introduction*, Second Edition, Springer-Verlag Berlin Heidenberg, 1991.

[93] L. Ley, S. P. Kowalczyk, F. M. McFeely, R. A. Pollak, and D. A. Shirley, *X-ray Photoemission fromnc: Evidence for Extra-Atomic Relaxation via Semilocalized Excitons*, Phys. Rev. B Vol 8 No 6 (1973) 2392.

[94] M. A. Brisk and D. A. Baker, *Shake-up Satellites in X-ray Photoelectron Spectroscopy*, J. Elec. Spec. Rel. Phen. 7 (1975) 197-213.

[95] K. Okada, A. Kotani, and B. T. Thole, *Charge Transfer Satellites and Multiplet Splitting in X-ray Photoemission Spectra of Late Transition Metal Halides*, J. Elec. Spec. Rel. Phen. 58 (1992) 325-343.

[96] K. S. Kim, *Charge Transfer Transition Accompanying X-ray Photoionization in Transition-Metal Compounds*, J. Elec. Spec. Rel. Phen. 3 (1974) 217-226.

[97] K. S. Kim and N. Winograd, *Charge Transfer Shake-up Satellites in X-ray Photoelectron Spectra of Cations and Anions of $SrTiO_3$, TiO_2 and Sc_2O_3*, Chemical Physics Letters, Vol.3 No 2 (1975) 312-317.

[98] H. Tillborg, A. Nilsson, and N. Mårtensson, *Shake-up and Shake-off Structures in Core Level Photoemission Spectra from Adsorbates*, J. Elec. Spec. Rel. Phen. 62 (1993) 73-93.

[99] P. W. Atkins, *Molecular Quantum Mechanics*, Second Edition, Oxford University Press, Oxford, 1983.

[100] W. Demtröder, *Atoms, Molecules and Photons*, Second Edition, Springer Heidelberg Dordrecht London New York, 2010.

[101] John C. Slater, *Quantum Theory of Matter*, Second Edition, McGraw-Hill, Inc. New York St. Louis San Francisco Toronto London Sydney, 1968.

[102] M. Sardela, *Practical Materials Characterization*, Springer New York Heidelberg Dordrecht London, 2014.

[103] John C. Slater, *Quantum Theory of Atomic Structure*, Volume I, McGraw-Hill, Inc. New York Toronto London, 1960.

[104] C. S. Fadley and D. A. Shirley, *Multiplet Splitting of Metal-Atom Electron Binding Energies*, Phys. Rev. A, Vol. 2, No. 4 (1970) 1109-1119.

[105] G. van der Laan, *Angular-Resolved Linear and Circular Dichroism in Core-Level Photoemission of Metalic Systems*, Phys. Rev. B Vol. 51, No 1 (1995) 240-248.

[106] C. Bethke, E. Kisker, N. B. Weber, and F. U. Hillebrecht, *Core-Valence Interactions in Cr and Fe 2p Photoemission*, Phys. Rev. B 71 (2005) 024413.

[107] F. Sirotti, M. De Santis, and G. Rossi, *Synchrotron-Radiation Photoemission and X-ray Absorption of Fe silicides*, Phys. Rev. B Vol 48 No 11 (1993) 8299-8305.

[108] F. Sirotti and G. Rossi, *Magnatic Asymmetry in Photoemission from Fe(100) with Linearly Polarized Synchrotron Radiation*, Phys. Rev. B Vol 49 No 22 (1994) 15682-15687.

[109] P. A. Cox, *The Electronic Structure and Chemistry of Solids*, Oxford Science Publications, Oxford, 1987.

[110] J. Stöhr, *NEXAFS Spectroscopy*, First Edition, Springer-Verlag, 1996.

[111] J. Stöhr, *X-ray Absorption: Principles, Applications, Techniques of EXAFS, SEXAFS and XANES*, R. Prins, Wiley New York, 1988, p.443.

[112] J. Stöhr, R. Jaeger, J. Feldhaus, S. Brennan, D. Norman, and G. Apai, *Extended absorption fine structure studies above the carbon, nitrogen, oxygen, and fluorine K absorption edges*, Applied Optics 19 (1980) 3911.

[113] J. Stöhr, *EXAFS and surface-EXAFS studies in the soft xray region using electron yield spectroscopy*, J. Vac. Sci. Tech. 16 (1979) 37.

[114] D. A. Outka, J. Stöhr, W. Jark, P. Stevens, J. Solomon, and R. J. Madix, *Orientation and bond length of molecular oxygen on Ag(110) and Pt(111): A near-edge x-ray-absorption fine-structure study*, Phys. Rev. B 35 (1987) 4119.

[115] J. Schnadt, J. Schiessling, J. N. O'Shea, S. M. Gray, L. Patthey, M. K. J. Johansson, M. Shi, J. Krempaský, J. Åhlund, P. G. Karlsson, P. Persson, N. Mårtensson, and P. A. Brühwiler, *Structural study of adsorption of isonicotinic acid and related molecules on rutile $TiO_2(110)$ I: XAS and STM*, Surf. Sci. 540 (2003) 39-54.

[116] L. Holland, *Vacuum Deposition of Thin Films*, Sixth Printing, Chapman and Hall Ltd., London, 1970.

[117] G. Lewin, *Fundamentals of Vacuum Science and Technology*, McGraw-Hill, Inc. New York St. Louis San Francisco Toronto London Sydney, 1965.

[118] I. W. Drummond, *Surface Analysis by Auger and X-ray Photoelectron Spectroscopy*, edited by D. Briggs and J.T. Grant, IM Publications and SurfaceSpectra Limited, 2003.

[119] D. R. Vij, *Handbook of Applied Solid State Spectroscopy*, Springer, New York, 2006.

[120] R. Nyholm, J. N. Andersen, U. Johansson, B. N. Jensen and I. Lindau, *Beamline I311 at MAX-lab: A VUV/Soft X-Ray Undulator Beamline for High Resolution Electron Spectroscopy*, Nuclear Instruments and Methods in Physics Research A 467-468 (2001) 520-524.

[121] J. Schnadt, J. Knudsen, J. N. Andersen, H. Siegbahn, A. Pietzsch, F. Hennies, N. Johansson, N. Mårtensson, G. Öhrwall, S. Bahr, S. Mähl, and O. Schaff, *The new ambient-pressure X-ray photoelectron spectroscopy instrument at MAX-lab*, J. Synchr. Rad. 19 (2012) 701-704.

[122] https://maxlab.lu.se (MAX-LAB - The MAX injector), accessed Oct. 27, 2014.

[123] Bastian Holst, Undulator, http://commons.wikimedia.org/wiki/File:Undulator.png, accessed Jan. 28, 2015.

[124] H. Winick, G. Brown, K. Halbach, and J. Harris, *Wiggler and Undulator Magnets*, Phys. Today, Vol 34 No 5 (1981) 50-63.

[125] M. Morkel, H. Unterhalt, M. Salmeron, G. Rupperechter, and H.-J. Freund, *SFG spectroscopy from 10^{-8} to 1000 mbar: less-ordered CO structures and coadsorption on Pd(111)*, Surf. Sci. 532-535 (2003) 103-107.

[126] G. Rupprechter and C. Weilach, *Spectroscopic Studies of Surface-Gas Interactions and Catalyst Restructuring at Ambient Pressure: Mind the Gap!*, J. Phys.: Conden. Matt. 20 (2008) 184019.

[127] H. Siegbahn, K. Siegbahn, J. Electron Spectrosc. Relat. Phenom. 2 (1973) 319.

[128] H. Siegbahn,*Electron-Spectroscopy For Chemical-Analysis Of Liquids And Solutions*, J. Phys. Chem. 89 (1985) 897.

[129] R. W. Joyner and M. W. Roberts, *A "High-Pressure" Electron Spectrometer for Surface Studies*, Surf. Sci. 87(1979) 501-509.

[130] D. F. Ogletree, H. Bluhm, G. Lebedev, C. S. Fadley, Z. Hussain, and M. Salmeron, *A Differentially Pumped Electrostatic Lens System for Photoemission Studies in the Millibar Range*, Rev. Sci. Inst. Vol 73 No 11 (2002) 3872-3877.

[131] V. Pérez-Dieste, L. Aballe, S. Ferrer, J. Nicolàs, C. Escudero, A. Milán, and E. Pellegrin, *Near Ambient Pressure XPS at ALBA*, J. .Phys.: Conf. Ser. 425 (2013) 072023.

[132] N. Johansson, Master thesis, Lund University, 2012.

[133] O. Snezhkova, F. Bischoff, Y. He, A. Wiengarten, S. Chaudhary, N. Johansson, K. Schulte, J. Knudsen, J. V. Barth, K. Seufert, W. Auwärter, J. Schnadt, *Iron phthalocyanine on Cu(111): coverage-dependent assembly and symmetry breaking, temperature-induced homocoupling, and modification of the adsorbate-surface interaction by annealing*, submitted to The Journal of Chemical Physics.

[134] O. Snezhkova, J. Lüder, A. Wiengarten, F. Bischoff, Y. He, S. R. Burema, J. Rusz, J. Knudsen, M.-L. Bocquet, K. Seufert, J. V. Barth, W. Auwärter, B. Brena, J. Schnadt, *Nature of the bias-dependent symmetry reduction of iron phthalocyanine on Cu(111)*, Physical Review B 92 (2015) 075428.

[135] http://www.nobelprize.org/nobel_prizes/physics/laureates/1986/press.html, accessed Feb. 19, 2015.

[136] G. Binnig and H. Rohrer, *Scanning tunneling microscopy*, Surface Science 126 (1983) 236.

[137] Gary Attard and Colin Barnes, *Surfaces*, Oxford University Press, Great Britain, 2004.

[138] L. Kuipers, R. W. M. Loos, H. Neerings, J. ter Horst, G.J. Ruwiel, A.P. de Jongh, and J. W. M. Frenken, *Design and Performance of a High-Temperature, High-Speed Scanning Tunneling Microscope*, Rev. Sci. Instr. 66 (1995) 4557.

[139] J. Wintterlin, J. Trost, S. Renisch, R. Schuster, T. Zambelli and G. Ertl, *Real-time STM observations of Atomic Equilibrium Fluctuations in an Adsorbate System: O/Ru(0001)*, Surf. Sci. 394 (1997) 159.

[140] C. Julian Chen, *Introduction to Scanning Tunnelling Microscopy*, Second Edition, Oxford Scholarship Online, 2007.

[141] G. Nimtz and A. Haibel, *Zero Time Space: How Quantum Tunnelling Broke the Light Speed Barrier*, Wiley-VCH, 2008.

[142] Elin Grånäs, *Above and Below Graphene: Nanoparticle Chemistry and Interface Reactions*, Ph. D. thesis, 2014 (p. 14).

[143] P. W. Hawkes, J. C. H. Spence (editors), and P. Sutter (contributor), *Science of Microscopy. Chapter: Scanning Tunnelling Microscopy in Surface Science*, Volume I, Springer Science+Business Media, LLC, 2007.

[144] F. Besenbacher, *Scanning Tunnelling Microscopy Studies of Metal Surfaces*, Rep. Prog. Phys. 59 (1996) 1737-1802.

[145] J. M. Gottfried, *Surface chemistry of porphyrins and phthalocyanines*, Surf. Sci. Rep. 70 (2015) 259-379.

[146] L. Gao, W. Ji, Y.B. Hu, Z.H. Cheng, Z.T. Deng, Q. Liu, N. Jiang, X. Lin, W. Guo, S.X. Du, W.A. Hofer, X.C. Xie, H. Gao, *Site-specific kondo effect at ambient temperatures in Iron-based molecules*, Phys. Rev. Lett. 99(10) (2007) 106402.

[147] X. Lu, K.W. Hipps, *Scanning tunneling microscopy of metal phthalocyanines: d6 and d8 cases*, J. Phys. Chem. B 101(27)(1997) 5391-5396.

[148] Z.H. Cheng, L. Gao, Z.T. Deng, Q. Liu, N. Jiang, X. Lin, X.B. He, S.X. Du, H. Gao, *Epitaxial growth of iron phthalocyanine at the initial stage on Au(111) surface*, J. Phys. Chem. C 111(6) (2007) 2656-2660.

[149] J. Åhlund, J. Schnadt, K. Nilson, E. Göthelid, J. Schiessling, F. Besenbacher, N.Mårtensson, C. Puglia, *The adsorption of iron phthalocyanine on graphite: a scanning tunnelling microscopy study*, Surf. Sci. 601(17) (2007) 3661-3667.

[150] A. Scarfato, S. Chang, S. Kuck, J. Brede, G. Hoffmann, R.Wiesendanger, *Scanning tunneling microscope study of iron(II) phthalocyanine growth on metals and insulating surfaces*, Surf. Sci. 602(3) (2008) 677-683.

[151] T.G. Gopakumar, T. Brumme, J. Krger, C. Toher, G. Cuniberti, R. Berndt, *Coverage-driven electronic decoupling of Fe-phthalocyanine from a Ag(111) substrate*, J. Phys. Chem. C 115(24) (2011) 12173-12179.

[152] N. Tsukahara, S. Shiraki, S. Itou, N. Ohta, N. Takagi, M. Kawai, *Evolution of kondo resonance from a single impurity molecule to the two-dimensional lattice*, Phys. Rev. Lett. 106(18) (2011) 187201.

[153] F. de Groot and A. Kotani, *Core Level Spectroscipy of Solids*, Boca Raton: Taylor & Francis Group, LLC, 2008.

[154] C. Isvoranu, J. Åhlund, B. Wang, K. Schulte, E. Ataman, N. Mårtensson, C. Puglia, J. N. Andersen, M. L. Bocquet, and J. Schnadt, *Electron spectroscopy study of the initial stages of iron phthalocyanine growth on highly oriented pyrolitic graphite*, J. Chem. Phys. 131 (2009) 214709.

[155] B. Brena, Y. Luo, M. Nyberg, S. Carniato, K. Nilson, Y. Alfredsson, J. Åhlund, N. Mårtensson, H. Siegbahn and C. Puglia, *Equivalent core-hole time-dependent density functional theory calculations of carbon 1s shake-up states of phthalocyanine*, Physical Review B 70 (2004) 195214.

[156] B. Brena and Y. Luo, *Time-dependent DFT calculations of core electron shake-up states of metal-(free)-phthalocyanines*, Radiation Physics and Chemistry 75 (2006) 1578-1581.

[157] Y. Bai, F. Buchner, M. T. Wendahl, I. Kellner, A. Bayer, Hans-Peter Steinrück, H. Marbach, and J. M. Gottfried, *Direct metalation of a phthalocyanine monolayer on Ag(111) with coadsorbed iron atoms*, J. Phys. Chem. C 112 (2008) 6087.

[158] K. Manandhar, K. T. Park, S.Ma, J. Hrbek, *Heteroepitaxial thin film of iron phthalocyanine on Ag(111)*, Surface Science 603 (2009) 636 - 640.

[159] K. Manandhar, T. Ellis, K. T. Park, T. Cai, Z. Song, J. A. Hrbek, *Scanning tunnelling microscopy study on the effect of post-deposition annealing of copper phthalocyanine thin films*, Surface Science 601 (2007) 3623 - 3631.

[160] A. Wiengarten, K. Seufert, W. Auwärter, D. Ecija, K. Diller, F. Allegretti, F. Bischoff, S. Fischer, D.A. Duncan, A.C. Papageorgiou, F. Klappenberger, R.G. Acres, T.N. Ngo, and J.V. Barth, *Surface-assisted dehydrogenative homocoupling of porphine molecules*, J. Am. Chem. Soc. 136 (2014) 9346 - 9354.

[161] I. Minkov, F. Gelmukhanov, H. Ågren, R. Friedlein, C. Suess, and W. R. Salaneck, *Core excitations of Biphenyl*, J. Phys. Chem. A 109 (2005) 1330 - 1336.

[162] T. Kravchuk, V. Venugopal, L. Vattuone, L. Burkholder, W. T. Tysoe, M. Smerieri, and M. Rocca, *Ethene Adsorption and Decomposition on the Cu(410) Surface*, J. Phys. Chem. C 113 (2009) 20881 - 20889.

[163] A. M. Goedken, S. L. Silva, S. M. York, and F.M. Leibsle, *STM Studies of the N/Cu(111) System: Surface Structure, Electron Confinement and Tip-Induced modification*, Eur. Phys. J. AP 19 (2002) 77-82.

[164] V. Higgs, P. Hollins, M. E. Premble, J. Pritchard, *Formation of a Surface Nitride On Copper(111) and its Influence on Carbon Monoxide Adsorption: Investigation by LEED, RAIRS And EELS*, J. Electron Spectrosc. Relat. Phenom. 39 (1986) 137.

[165] A. Soon, L. Wong, M. Lee, M. Todorova, B. Delley, C. Stampfl, *Nitrogen adsorption and thin surface nitrides on Cu(111) from first-principles*, Surf. Sci. 601 (2007) 4775 - 4785.

[166] J. F. Skelly, T. Bertrams, A. W. Munz, M. J. Murphy, A. Hodgson, *Nitrogen induced restructuring of Cu(111) and explosive desorption of N_2*, Surface Science 415 (1998) 48-61.

[167] M. A. Muñoz-Márquez, G. S. Parkinson, P. D. Quinn, M. J. Gladys, R. E. Tanner, D. P. Woodruff, T. C. Q. J. Noakes, P. Bailey, *N-induced pseudo-(100) reconstruction of Cu(111): One layer or more?*, Surf. Sci. 582 (2005) 97-109.

[168] J. T. Hoeft, M. Polcik, M. Kittel, R. Terborg, R. L. Toomes, J. Kang, *Photoelectron diffraction structure determination of Cu(100)c(2×2)-N*, Surf. Sci. 492 (2001) 1-10.

[169] B. Warner, F. El Hallak, H. Prüser, J. Sharp, M. Persoon, A. J. Fisher, C. F. Hirjibehedin, *Tunable magnetoresistance in an asymmetrically coupled single-molecule junction*, Nature Nanotechnology 10 (2015) 259 - 263. (supplementary information)

[170] I. Bidermane, J. Lüder, R. Totani, C. Grazioli, M. de Simone, M. Coreno, A. Kivimäki, J. Åhlund, L. Lozzi, B. Brena, and C. Puglia, *Characterization of gas phase iron phthalocyanine with X-ray photoelectron and absorption spectroscopies*, Phys. Status Solidi B 252 No. 6 (2015) 1259-1265.

[171] B. Eren, C. Heine, H. Bluhm, G. A. Somorjai, and M. Salmeron, *Catalyst Chemical State during CO Oxidation Reaction on Cu(111) Studied with Ambient-Pressure Xray Photoelectron Spectroscopy and Near Edge Xray Adsorption Fine Structure Spectroscopy*, J. Am. Chem. Soc. 137 (2015) 11186-11190.

[172] B. Eren, L. Lichtenstein, C. Hao Wu, H. Bluhm, G. A. Somorjai, and M. Salmeron, *Reaction of CO with Preadsorbed Oxygen on Low-Index Copper Surfaces: An Ambient Pressure Xray Photoelectron Spectroscopy and Scanning Tunneling Microscopy Study*, J. Phys. Chem. C 119 (2015) 14669-14674.